NASA CONTRACTOR REPORT


NASA CR-2343

NASA CR-2343

# THE RADIOMETER TRANSFER FUNCTION FOR THE AAFE COMPOSITE TWO-FREQUENCY RADIOMETER SCATTEROMETER

*by J. H. Moore*

*Prepared by*
GENERAL ELECTRIC COMPANY
Philadelphia, Pa.
*for Langley Research Center*

NATIONAL AERONAUTICS AND SPACE ADMINISTRATION • WASHINGTON, D. C. • DECEMBER 1973

| 1. Report No. | 2. Government Accession No. | 3. Recipient's Catalog No. |
|---|---|---|
| NASA CR-2343 | | |

| 4. Title and Subtitle | 5. Report Date |
|---|---|
| The Radiometer Transfer Function for the AAFE Composite Two-Frequency Radiometer Scatterometer | December 1973 |
| | 6. Performing Organization Code |

| 7. Author(s) | 8. Performing Organization Report No. |
|---|---|
| J. H. Moore | |
| | 10. Work Unit No. |
| 9. Performing Organization Name and Address | |
| General Electric Company<br>Philadelphia, PA | 11. Contract or Grant No. |
| | 13. Type of Report and Period Covered |
| 12. Sponsoring Agency Name and Address | Contractor Report |
| National Aeronautics and Space Administration<br>Washington, DC 20546 | 14. Sponsoring Agency Code |

15. Supplementary Notes This is a topical report. The information presented herein was offered as a thesis in partial fulfillment of the requirements for the degree of Master of Science in Engineering, University of Pennsylvania, August 1973.

16. Abstract

A model was developed for the switching radiometer utilizing a continuous method of calibration. Sources of system degradation were identified and include losses and voltage standing wave ratios in front of the receiver input. After computing the three modes of operation (Baseline Calibration, Normal Calibration, and Measurement Mode), expressions were developed for the normalized radiometer output, the minimum detectable signal (normalized RMS temperature fluctuation), sensitifity (Figure of Merit), and accuracy correction factors).

The results compared favorably with the predicted performance of the instrument using the expressions developed herein.

| 17. Key Words (Suggested by Author(s)) | 18. Distribution Statement |
|---|---|
| Microwave radiometer<br>RADSCAT<br>Feedback Radiometer | Unclassified - Unlimited |

| 19. Security Classif. (of this report) | 20. Security Classif. (of this page) | 21. No. of Pages | 22. Price* |
|---|---|---|---|
| Unclassified | Unclassified | 76 | Domestic, $3.75<br>Foreign, $6.25 |

*For sale by the National Technical Information Service, Springfield, Virginia 22151

TABLE OF CONTENTS

LIST OF FIGURES

LIST OF TABLES

# SECTION 1
# INTRODUCTION

A Composite Two-Frequency Radiometer-Scatterometer (RADSCAT) has been designed and developed to infer the earth-surface wind and sea state through remote measurements and analysis of both the radar differential scattering cross section and the microwave emission of the sea surface using active and passive microwave sensors. Both the scatterometer and the radiometer are complex sensors requiring extensive testing and evaluation of the test data. Models of the earth's surface must also be developed and analyzed. To date, at least eighty-six papers and reports on the subject of the ocean surface have been compiled by Tomiyasu[1]. This compilation is not considered to be comprehensive nor all inclusive but serves to illustrate the wide variety of thought and areas to be analyzed in considering the models of the ocean surface alone.

The Advanced Applications Flight Experiment (AAFE) RADSCAT was designed to collect radiometer and scatterometer data over the ocean in a quasi simultaneous manner, the following being the parameters of interest:

- Frequency
- Antenna Polarization
- Altitude (Antenna footprint)
- Incidence Angle
- Wind direction

Such data, once acquired, would then be used by NASA and its contractors to (1) serve as data in existing models of the ocean surface and (2) serve to provide more information for the formulation of new or improved models of the sea and wind relationships.

As a specific example, the University of Kansas[2] has earmarked the use of RADSCAT for wind measurements and precipitation sensing in the area of Meteorology. In Oceanography, wave forecasting and arctic ice movements will be measured. In Hydrology, soil moisture content, snowfield mapping, and freeze-thaw line detection are to be sensed and measured. The University of Kansas experiment objectives are three in number:

- Determine the accuracy of wind speed estimates from joint microwave observations.
- Determine operational characteristics for a spacecraft-oriented wind measuring system with regard to frequency, view angles and polarization.
- Determine cloud and rain effects on radiometer data, scatterometer data with respect to path attenuation, rainfall rate and areas, and the effects of rain impact on the measured surface.

From the RADSCAT experiment and data collection a composite theory of microwave emissions and backscatter is to be developed.

The RADSCAT instrument, Figure 1-1, is a composite radiometer and scatterometer sharing a common antenna, RF front end and IF strip, but

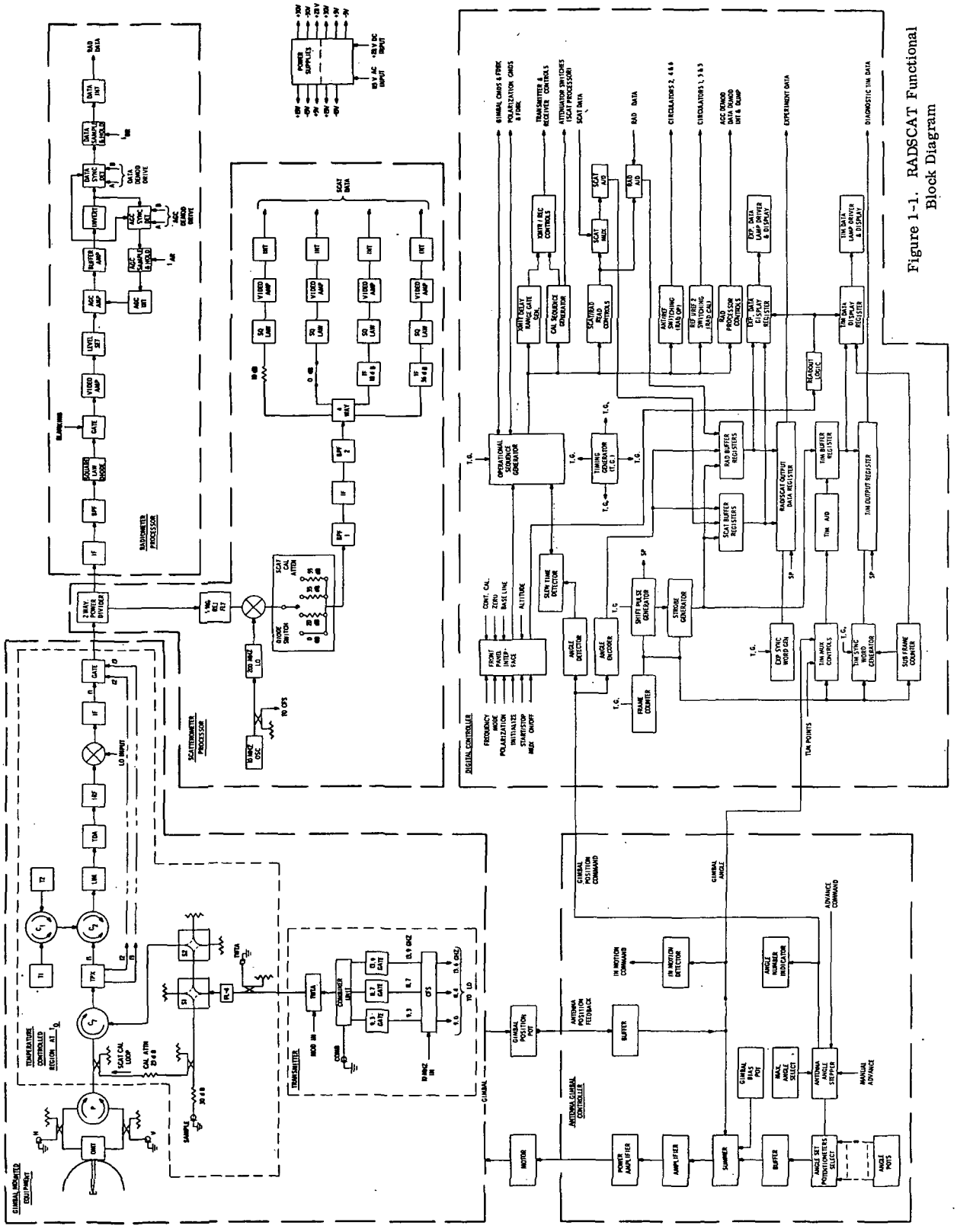

Figure 1-1. RADSCAT Functional Block Diagram

having two separate signal processors. The antenna is a mechanically scanned, pencil beam, dual polarization device with high beam efficiency and low side lobe levels. Sharing a common antenna allows RADSCAT to perform radiometric and scatterometric measurements in sequence on the same ground cell without the problem of the alignment of two separate antennas. Mounting the sensitive RF receiver components on the rear of the antenna and allowing only the high level IF signals to cross the moveable interface eliminated the need for flexible waveguides or rotary joints at points in the system (such as the receiver input) where those devices could introduce variations in signal strength which would degrade the performance of the instrument. A prime example of the possible degradation in performance is in the radiometer where any change in loss before the Dicke switch introduces a direct error to the measured brightness temperature.

The receiver consists of three independent (two used currently) front ends and downconverters. The microwave input is channeled to the proper amplifier-downconverter chain by a triplexing device and the proper IF is selected by a channel selection switch. Separate processors are used to convert the IF signal to radiometer and scatterometer data outputs. A digital controller (mini computer) controls all timing and operational sequences as well as digitalizing and formating the data.

The radiometer subsystem of RADSCAT is a very sensitive radiometer using two reference loads. The two reference loads are used to continuously

calibrate and stabilize the radiometer by means of an AGC loop. The radiometer is a form of the Dicke[3] radiometer, i.e., it alternately switches a sensitive receiver between the antenna and a reference temperature (Dicke temperature). However, the RADSCAT reference temperature consists of two reference terminations at different temperatures which are alternately switched into the role of the Dicke temperature. This results in an equivalent Dicke temperature equal to the average of the two reference temperatures. With suitable signal processing a signal proportional to the difference between these two reference temperatures is developed and used to control the radiometer system gain. The long-term stability of the calibration of this radiometer system is more than one order of magnitude better than the usual Dicke radiometer, while reducing the sensitivity by only a factor of two.

## SECTION 2

## THE DUAL REFERENCE TEMPERATURE RADIOMETER

The Dual Reference Temperature Radiometer was originally proposed by Weinreb[4] using a digital computer for continuous calibration, as well as gain and noise temperature monitoring by a real-time data analysis of the radiometer output. Hach[5] proposed a self-contained continuously calibrated radiometer needing no external computer. Both Hach[6] and Louapre[7] have constructed such radiometers with good results.

By sequentially switching a low noise receiver between the antenna and reference terminations and detecting the resulting receiver noise power by means of a square law detector a waveform whose peak levels are proportional to temperature results. Synchronously detecting these peak levels derives a measure of the antenna brightness temperature as well as a measure of the system gain. Using a feedback loop, the measure of system gain is applied to an AGC amplifier to maintain a constant system gain. Once the gain of the system is made constant, the radiometer calibration does not change, i.e., a continuously calibrated radiometer results.

Figure 2-1 is the radiometer subsystem block diagram showing the key components and interfaces found in the RADSCAT instrument. Table 2-1 is a list of symbols and abbreviations which are used in the general description and analysis of the radiometer.

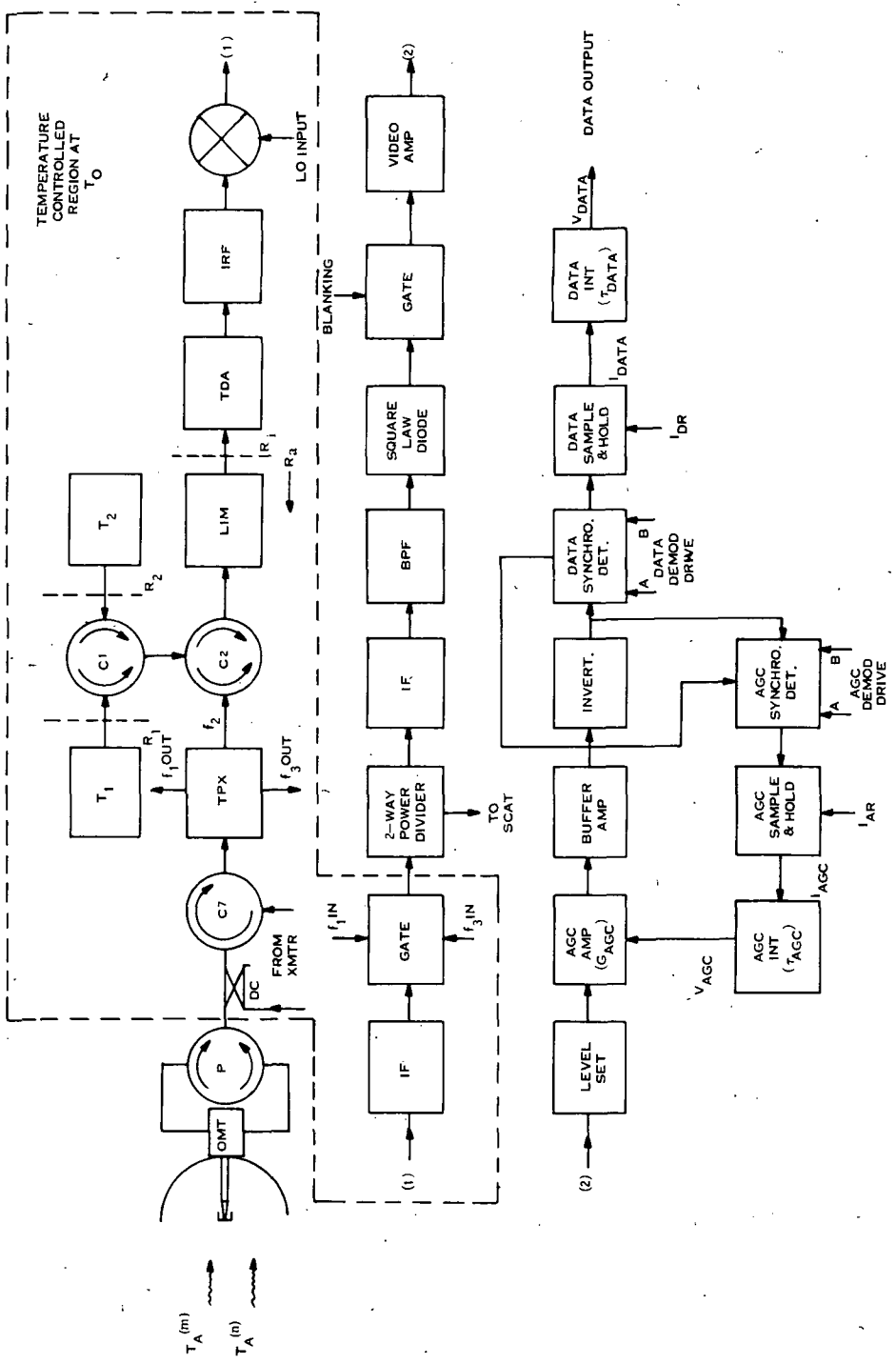


Figure 2-1. Radiometer Subsystem Block Diagram

Table 2-1. List of Symbols and Abbreviations

| | |
|---|---|
| AGC | Automatic Gain Control |
| BPF | Bandpass Filter to define radiometer's bandwidth |
| C1 | Reference termination switching circulator ($\Delta T$ switch) |
| C2 | Dicke circulator (Dicke switch) |
| C7 | Transmit Receive (T-R) circulator |
| $C_{mm}$ | Power coupling coefficient between $m^{th}$ and $n^{th}$ polarization in antenna subsystem, $m^{th}$ polarization selected |
| CCR | Continuously Calibrated Radiometer |
| DC | Directional Coupler |
| $f_1, f_2, f_3$ | Frequencies of operation, or frequency channel |
| FET | Field Effect Transistor |
| GATE | Range gate and channel selection switch |
| $G_{AGC}$ | AGC amplifier gain |
| IF | Intermediate frequency amplifier |
| IRF | Image Rejection Filter |
| $L_i$ | Loss of the $i^{th}$ component |
| $L_{mm}$ | Antenna loss with respect to $m^{th}$ polarization |
| LIM | Power limiter for TDA protection |
| OMT | Orthogonal Mode Transducer |
| P | Polarization switch or circulator |

Table 2-1. List of Symbols and Abbreviations (Cont)

| | |
|---|---|
| $R_i$ | Power reflection coefficient at $i^{th}$ reference plane or of $i^{th}$ component |
| $R_{mm}$ | Antenna power reflection coefficient with respect to $m^{th}$ polarization |
| RMS | Root mean square |
| $T_1$ | Temperature of reference termination No. 1 |
| $T_2$ | Temperature of reference termination No. 2 |
| $T_{1e}$ | Effective temperature of reference termination No. 1 referred to receiver input |
| $T_{2e}$ | Effective temperature of reference termination No. 2 referred to receiver input |
| $T_A$ | Antenna brightness temperature |
| $T_A^{(m)}$ | Antenna brightness temperature when $m^{th}$ polarization is selected |
| $T_A^{(n)}$ | Antenna brightness temperature when $n^{th}$ polarization is selected |
| $T_{Ae}^{(m)}$ | Effective antenna temperature at input to receiver when $m^{th}$ polarization is selected |
| $T_F$ | Physical temperature of antenna and feed system |
| $T_i$ | Temperature of the $i^{th}$ component |
| $T_P$ | Physical temperature of polarization switch |
| $T_R$ | Effective receiver noise temperature |
| $T_o$ | Physical temperature of thermally controlled oven |
| TDA | Tunnel Diode Amplifier |

Table 2-1. List of Symbols and Abbreviations (Cont)

| | |
|---|---|
| TPX | Triplexer |
| VSWR | Voltage Standing Wave Ratio |
| X | Mixer |
| $\epsilon$ | Blanking period |
| $\xi$ | Normalized radiometer output |
| $\tau$ | DATA period |
| $\Gamma$ | Complex reflection coefficient |

The timing diagrams are shown in Figures 2-2, 2-3, 2-4. While the operation of the Dicke and $\Delta T$ switches are relatively straight forward and apparent from Figure 2-2 (composite video) the synchronous detection function in the radiometer processor needs additional explanation.

The radiometer processor is a multifunction assembly whereby the composite video signal from the RF subsystem is amplified, demodulated, and applied to an integrate-and-dump filter. Its major components are: amplifier circuitry, demodulation circuitry, integration-and-dump network. During normal operation (or antenna modulation) the level set attenuator shown in Figure 2-1 is used (in conjunction with AGC bias control) to adjust for the proper signal level in the AGC circuit, and at the DATA integrator output. Variable gain for AGC purposes is achieved with a field effect transistor (FET, used as a controllable resistance) as one of the feedback loop elements of an operational amplifier. Following the AGC amplifier is a fixed-gain operational amplifier where the composite signal is amplified in preparation for demodulation. The inverter is used to derive a complementary signal for full-wave synchronous demodulation. Full-wave synchronous demodulation is achieved through the use of dual FET switches, both for the AGC signal and for the DATA signal.

The AGC demodulated signal current is applied to the AGC error amplifier and summed with current from a zener regulated reference voltage supply. The difference current is sensed by the amplifier which operates

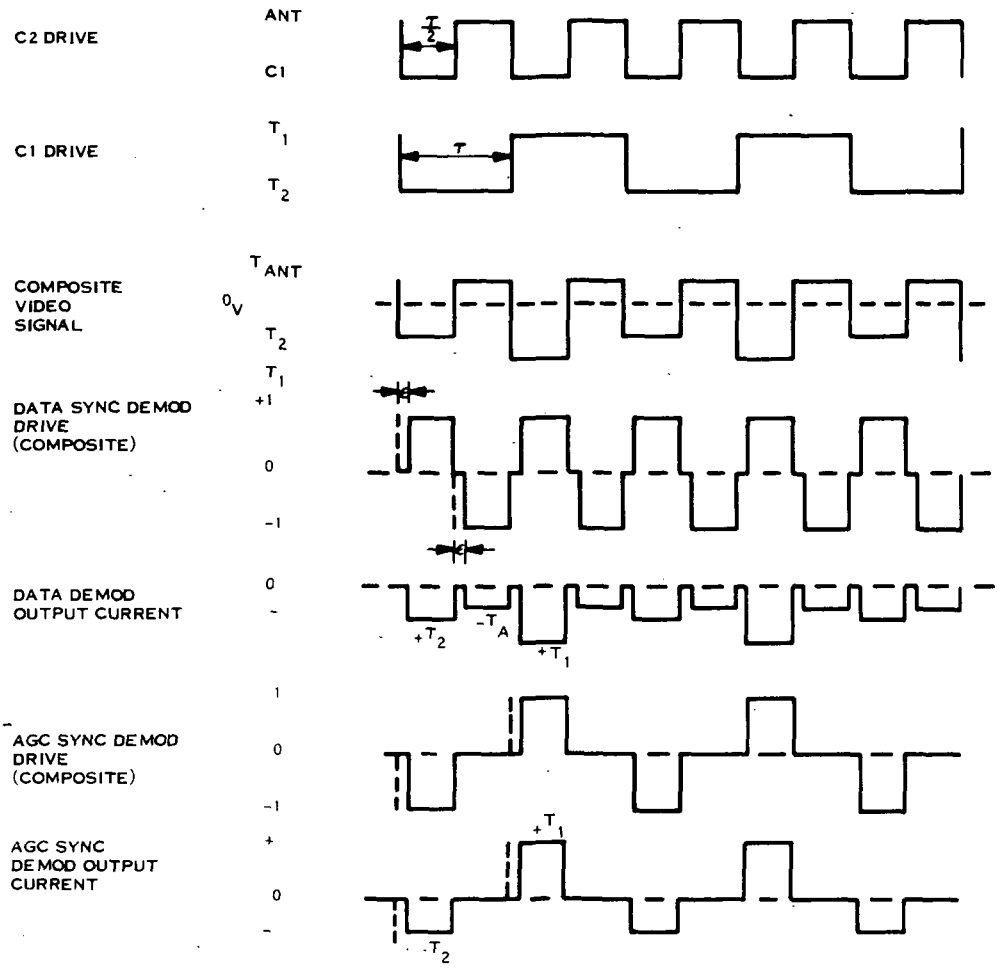


Figure 2-2. Timing - Antenna Measurement Mode

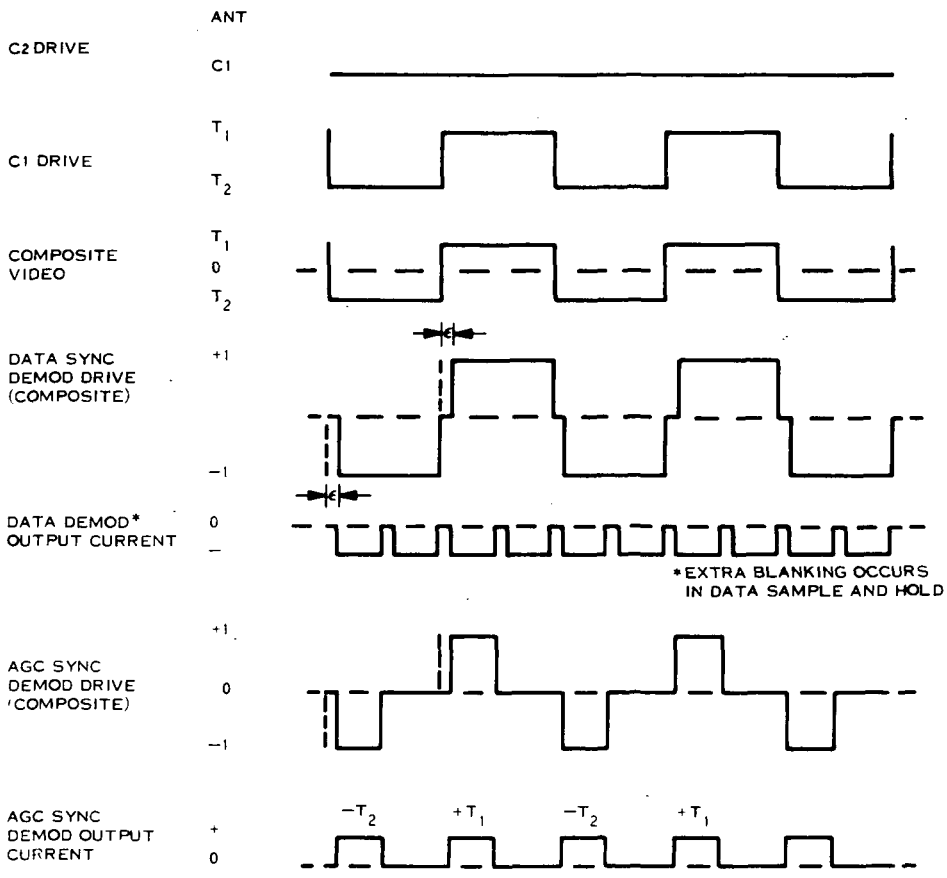


Figure 2-3. Timing - Calibration Mode

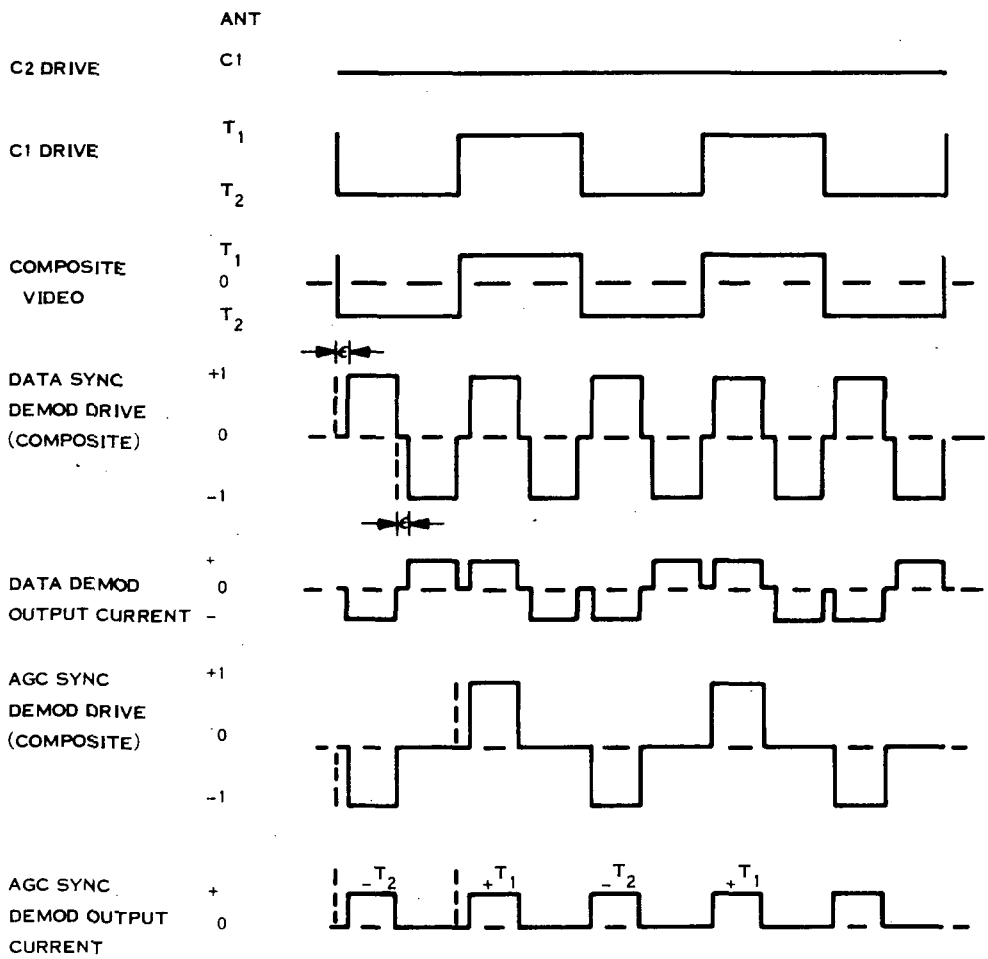


Figure 2-4. Timing - Baseline Calibration Mode

open loop (high gain) and in a low pass filter (integrator) mode to smooth the demodulated signal fluctuations. The voltage developed by the error amplifier is the control voltage for the variable gain element. The signal from the DATA demodulator is applied to the integrate-and-dump filter, with a dual FET switch performing the sample-hold-dump functions.

In the radiometer calibration mode the DATA channel produces a voltage proportional to the difference between the two reference load temperatures. In the baseline mode, a composite video waveform is generated such that after detection by the DATA demodulator a zero output voltage results. This technique is used to detect any system offset or bias. An intentional bias is applied to the DATA integrator so that the baseline is offset from zero for diagnostic purposes.

A detailed analysis of the three modes of operation of the radiometer and processor will be covered in Section 5.

## SECTION 3

## STATEMENT OF THE PROBLEM AND AN OUTLINE OF THE SOLUTION

The need to express the system transfer function explicitly stems from the desire of the ultimate user of the system to relate the output of the system to the input parameters. From a pragmatic point of view, the system is of no use unless it is predictable and accurate to within some predetermined tolerance. Ideally, the output should be directly proportional to the input with no errors. However, physical systems are not ideal and the sources of error must therefore be identified. So it is with the dual reference temperature radiometer. The radiometer transfer function is a combination of many subassembly transfer functions, each with its own sources of error. Errors combine in random as well as predictable ways when the subassemblies are integrated. To determine the system error, the individual transfer functions must be determined, combined, and analyzed.

As the case in point, the radiometer relies upon timing, reference terminations, antenna, detection, and processing subassemblies to accomplish the task of measuring radiometric temperature. Because the RADSCAT instrument was a dual-purpose, multi-frequency unit with a compact design, the losses and VSWR's in the system were higher than if individual single function instruments were constructed. Predicted instrument performance estimates prior to construction did not take into account the higher losses and VSWR's which were realized in the construction of the instrument.

As a result, the radiometer as finally configured did not meet its predicted performance. The radiometer prediction model had been based upon an analysis similar to Hach's[6]. However, as noted before, the low loss-low VSWR constraints of that analysis were violated. Therefore a more general solution for the dual reference temperature radiometer transfer function and the expressions for sensitivity, accuracy and resolution had to be found.

The solutions to these problems, the topic of this thesis, will proceed from a simple model of a noise measuring system to the more complex model of a switching radiometer. A model of the RADSCAT radiometer will be developed and a solution based upon the internal (continuous) calibration will be found for the general case. Expressions for the resolution, accuracy and sensitivity (Figure of Merit) will be developed. The quantities are to be expressed as RMS estimates as a function of antenna brightness temperature.

SECTION 4

GENERAL SOLUTION

## 4.1 SIMPLE MODEL

For the analysis of a radiometer we shall assume a uniform spectral noise power density from the noise sources across the bandwidth of interest so that the measuring system's bandwidth is the bandwidth limiting element in the measurement analysis.

The available power[8, 9] from a network is

$$P_a = KTB \tag{1}$$

where K is Boltzmann's constant, B is the effective bandwidth, and T is the available temperature. For the purpose of simplifying the radiometer analysis, "temperature" will also be used synonymously with "noise power" though it is a sloppy but common notation. It should also be remembered that a device may have an equivalent noise power, T, not directly related to its physical temperature, i.e., active devices may have noise temperatures of many thousands of degrees Kelvin yet be no warmer than room temperature. Figure 4-1 is a simple radiometer. A noise source, $T_S$, is connected to the input of a sensitive receiver via a lossy two-port ($\alpha_S$, $T_L$). Using the analysis from Appendix A, it is possible to express the power delivered, NT, across reference plane 2 to the receiver.

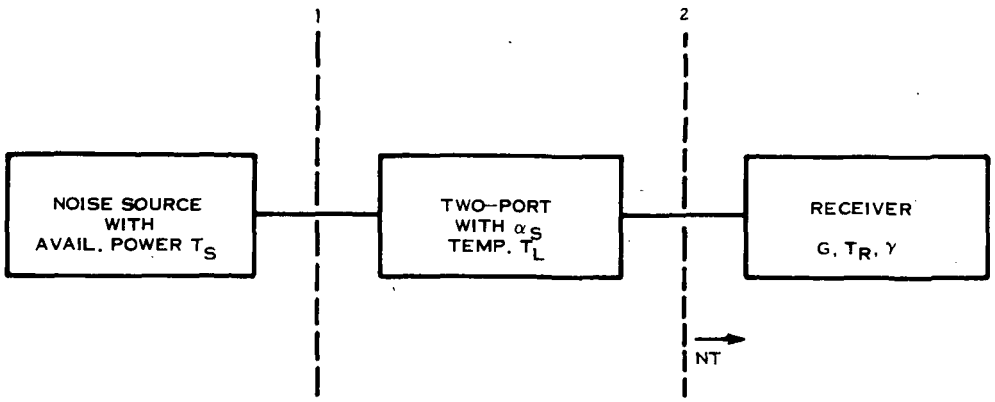


Figure 4-1. Simple Radiometer

In general,

$$NT = M\eta\, T_S + N\, T_L\, (1 - \alpha_S) \tag{2}$$

$$= N\, (T_S\, \alpha_S + T_L\, (1 - \alpha_S)) \tag{3}$$

With a matched output, (N = 1),

$$T = T_S\, \alpha_S + T_L\, (1 - \alpha_S) \tag{4}$$

and if lossless, ($\alpha_S = 0$),

$$T = T_S \tag{5}$$

As can be seen from equation 3, both output mismatch and device loss affect the amount of available noise power transferred to the receiver and, as will be shown later, are direct sources of error in radiometric measurements.

Carrying the analysis through the receiver, the output of the radiometer may be expressed as,

$$I_{OUT} = KBG\gamma\,(NT_S + T_R) \tag{6}$$

where

K is Boltzmann constant
NT is defined by equation 2
B is the receiver bandwidth
G is the receiver gain
$\gamma$ is a constant embodying detector constants
$T_R$ is the receiver noise temperature

The output of such a radiometer will be greatly influenced by any variations in G, B, $\gamma$, $T_R$. Such problems led Dicke[10] to develop the switching radiometer.

## 4.2 SWITCHING RADIOMETER

Figure 4-2 is a generalized switching radiometer. Again applying the analysis of Appendix A,

$$(N_1\,T)_S = N_1\,[T_S\,\alpha_S + T_L\,(1 - \alpha_S)\,] \tag{7}$$

$$(N_2\,T)_X = N_2\,[T_X\,\alpha_X + T_L\,(1 - \alpha_X)\,] \tag{8}$$

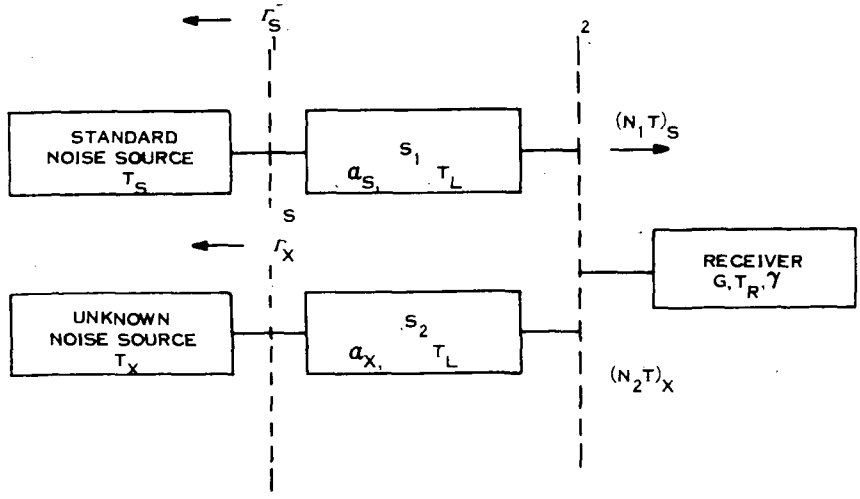


Figure 4-2. Switching Radiometer

The receiver is alternately switched between the known and unknown sources and, with suitable processing, the receiver output is proportional to the difference in the source temperatures.

The receiver output may be expressed as

$$I_{OUT} = KGB\gamma \left[ (N_1 T)_S - (N_2 T)_X \right]$$

$$= KGB\gamma \left[ N_1 \left( T_S \alpha_S + T_L (1 - \alpha_S) \right) \right.$$

$$\left. - N_2 \left( T_X \alpha_X + T_L (1 - \alpha_X) \right) \right] \quad (9)$$

$$I_{OUT} = KGB\gamma \left[ N_1 T_S \alpha_S - N_2 T_X \alpha_X \right.$$

$$\left. + T_L (N_1 - N_2 + \alpha_X N_2 - \alpha_S N_1) \right] \quad (10)$$

If $N_1 = N = N_2$, then

$$I_{OUT} = KGB\gamma N \left( T_S \alpha_S - T_X \alpha_X + T_L (\alpha_X - \alpha_S) \right] \quad (11)$$

and also if $\alpha_S = \alpha = \alpha_X$, then

$$I_{OUT} = KGB\gamma N \alpha \left[ T_S - T_X \right] \quad (12)$$

Equation 12 illustrates the ideal case for the switching radiometer where the output of the radiometer is proportional to the difference in the two temperatures and independent of the receiver noise. The only constraint on the receiver is that the short term stability be sufficiently good for the duration of the switching period. However, the long term gain variations of the receiver still must be considered when evaluating the radiometer accuracy. Also, as may be seen from equation 10, any difference in mismatches $N_1$, $N_2$ or losses $\alpha_1$, $\alpha_2$ result in receiver noise contribution to the radiometer output degrading the performance of the radiometer.

If, however, a second reference temperature is used and the receiver processes the inputs so that there are two outputs, $I_{AGC}$ (proportional to the difference of the two reference temperatures) and $I_{DATA}$ (proportional to the difference between the unknown temperature and the average of the reference temperatures, then the long term gain stability of the receiver would no longer enter into the measurement.

Let

$$I_{DATA} = KGB\gamma N\alpha \left[ \frac{T_{S1} + T_{S2}}{2} - T_X \right] \tag{13}$$

and $$I_{AGC} = KGB\gamma N\alpha \left[ T_{S1} - T_{S2} \right] \tag{14}$$

Solving (14) for G,

$$G = \frac{I_{AGC}}{KB\gamma N\alpha \left( T_{S1} - T_{S2} \right)} \tag{15}$$

and using $I_{AGC}$ to control the receiver gain,

$$I_{DATA} = \frac{\left[ T_{S1} + T_{S2} - 2T_X \right] I_{AGC}}{2 \left[ T_{S1} - T_{S2} \right]} \tag{16a}$$

or

$$\frac{I_{DATA}}{I_{AGC}} = \frac{\left[ T_{S1} + T_{S2} - 2T_X \right]}{2 \left[ T_{S1} - T_{S2} \right]} \tag{16b}$$

Equations 16(a, b), then, are the basis for the ideal dual reference temperature (or continuously calibrated) radiometer.

## 4.3 ANALYSIS OF THE DUAL REFERENCE TEMPERATURE (OR CONTINUOUSLY CALIBRATED) RADIOMETER

Equation 16a is a very idealized expression for the continuously

calibrated radiometer (CCR). If we extend the non-ideal analysis of the switching radiometer to include two temperature references we find

$$I_{DATA} = \frac{1}{2} KGB\gamma \left[ (N_1 T)_{S1} + (N_2 T)_{S2} - 2 (N_3 T)_X \right] \quad (17)$$

$$I_{AGC} = KGB\gamma \left[ (N_1 T)_{S1} - (N_2 T)_{S2} \right] \quad (18)$$

Expanding (17) and (18)

$$I_{DATA} = \frac{1}{2} KGB\gamma \left[ N_1 (T_{S1} \alpha_S + T_R (1 - \alpha_{S1})) + N_2 (T_{S2} \alpha_{S2} + T_R (1 - \alpha_{S2})) - 2 N_3 (T_X \alpha_X + T_R (1 - \alpha_X)) \right] \quad (19)$$

$$I_{AGC} = KGB\gamma \left[ N_1 (T_{S1} \alpha_{S1} + T_R (1 - \alpha_{S1})) - N_2 (T_{S2} \alpha_{S2} + T_R (1 - \alpha_{S2})) \right] \quad (20)$$

and substituting (20) into (19) after solving for G we find

$$I_{DATA} = I_{AGC} \left[ N_1 (T_{S1} \alpha_{S1} + T_R (1-\alpha_{S1})) + N_2 (T_{S2} \alpha_{S2} + T_R (1 - \alpha_{S2})) - N_3 (T_X \alpha_X + T_R (1 - \alpha_X)) \right] \div \left[ 2 \left[ N_1 (T_{S1} \alpha_{S1} + T_R (1 - \alpha_{S1})) - N_2 (T_{S2} \alpha_{S2} + T_R (1 - \alpha_{S2})) \right] \right] \quad (21)$$

As can be seen from equation 21, the gain, bandwidth, and detector constants common to both the $I_{DATA}$ and $I_{AGC}$ expressions have again been eliminated from the expression for the radiometer output, $I_{DATA}$. However,

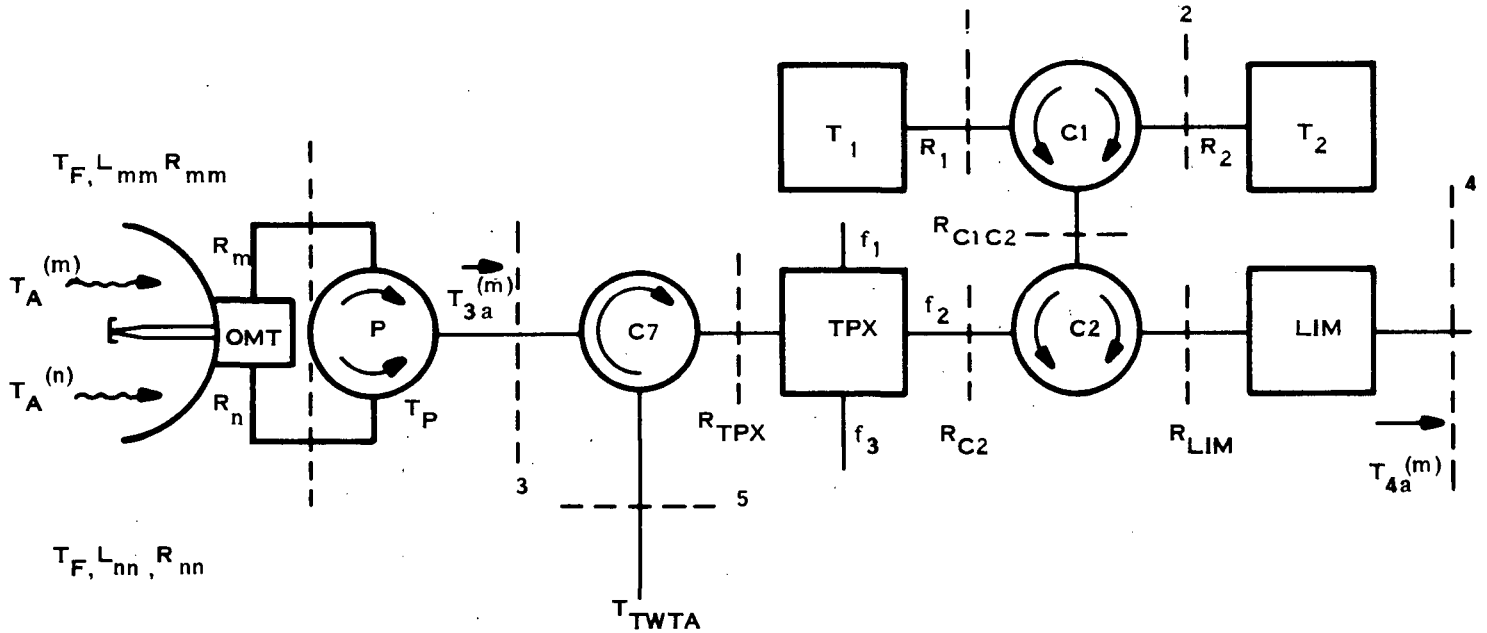


Figure 4-3. Simplified RADSCAT Radiometer Block Diagram

a portion of the receiver noise temperature, $T_R$, has been introduced into the output by the terms $(1 - \alpha_{S1})$, $(1 - \alpha_{S2})$, and $(1 - \alpha_X)$. The magnitude of these terms, as will be shown later in Section 4.10, may greatly influence the contribution of receiver noise fluctuations into the radiometer output.

Using the RADSCAT radiometer block diagram for the model of the continuously calibrated radiometer, an exact analysis of the CCR will be undertaken. Direct noise injection into the receiver, via the TWTA, along with the cross polarization input due to the antenna system will be accounted for. Figure 4-3 is a simplified radiometer system block diagram which will be used to analyze the CCR. It divides the CCR into functional groups with practical interfaces to facilitate the analysis.

## 4.4 SOURCES OF SYSTEM DEGRADATION

Referring to Figure 4-3, sources of system degradation due to noise, VSWR, or loss will be identified so that these sources may be explicitly identified in the analysis of the CCR.

Starting with the antenna subassembly, the antenna pattern, VSWR, losses and cross polarization components must be considered. The polarization selection switch, P, has VSWR, loss, and finite isolation which must be taken into account. TWTA noise enters into the receiver via C7, the T-R circulator. The reference temperature terminations $T_1$, $T_2$, and $\Delta T$ switch, C1, with their composite VSWR, loss, and isolation introduce potential errors into the reference arm of the radiometer. The Dicke switch, C2, and the protection limiter, LIM, introduce loss and VSWR into the signal

path. Also, these terms are different for the reference and measurement arms of the radiometer depending upon the positions of C1, C2. The receiver and processor (i.e., TDA through DATA integrator) introduce noise into the measurements. Other sources of performance degradation include timing variations, short-term thermal variations in lossy elements, and power supply variations coupled into the reference voltages.

## 4.5 DEFINITION OF REFERENCE PLANES

There are seven reference (or interface) planes of interest in the simplified radiometer system block diagram, shown in Figure 4-3. While all seven will not be explicitly treated in the analysis, they provide a convenient way to break the system into functional groupings of components. Reference plane 1 is the interface of reference temperature 1 and the associated port of the $\Delta T$ switch, C1. Reference plane 2 is similarly associated with reference temperature 2. Reference plane 3 is the interface between the antenna subassembly and the receiver input. Reference plane 4 is defined as the input to the receiver. Reference plane 5 is the interface between the TWTA and the T-R circulator, C7. Not shown in Figure 4-3 are Reference plane 6, the local oscillator input interface, and reference plane 7, the IF output to the processing electronics.

## 4.6 SUBASSEMBLY TRANSFER FUNCTIONS

The analysis will proceed by generating individual subassembly transfer functions starting first with the antenna. Consider first the following definitions. Let $R_i$ be the composite power reflection coefficient at the $i^{th}$

reference plane, $L_i$ the loss ($0 \leq L_i \leq 1$) and $T_i$, the temperature of the $i^{th}$ component. Starting with the model in Figure 4-4, excerpted from Figure 4-3, the antenna subassembly transfer-function shall be generated.

$T_{3a}^{(m)}$ is the maximum available power, with the $m^{th}$ polarization selected, at reference plane 3. $T_{3a}^{(m)}$ consists of four main sources of power:

$T_A^{(m)}$ - The desired polarization signal

$T_A^{(n)}$ - The undesired polarization signal

$T_F$ - The ambient temperature of the feed and OMT.

$T_P$ - The ambient temperature of the polarization switch.

Combining these sources of power with respect to the network of Figure 4-4 gives the result

$$\begin{aligned} T_{3a}^{(m)} = {} & T_A^{(m)} \left[ L_{mm} (1 - R_{mm}) L_P (1 - R_m) \right. \\ & \left. + L_{mm} (1 - R_{mm}) C_{mn} (1 - R_n) L_P^2 R_m \right] \\ & + T_A^{(n)} \left[ L_{nn} (1 - R_{nn}) C_{mn} L_P (1 - R_m) \right. \\ & \left. + L_{nn} (1 - R_{nn}) L_P^2 (1 - R_n) R_m \right] \\ & + T_F \left[ (1 - L_{mm}) (1 - R_m) L_P \right. \\ & \left. + (1 - L_{nn}) (1 - R_n) L_P^2 R_m \right] \\ & + T_P (1 - L_P) \end{aligned} \tag{22}$$

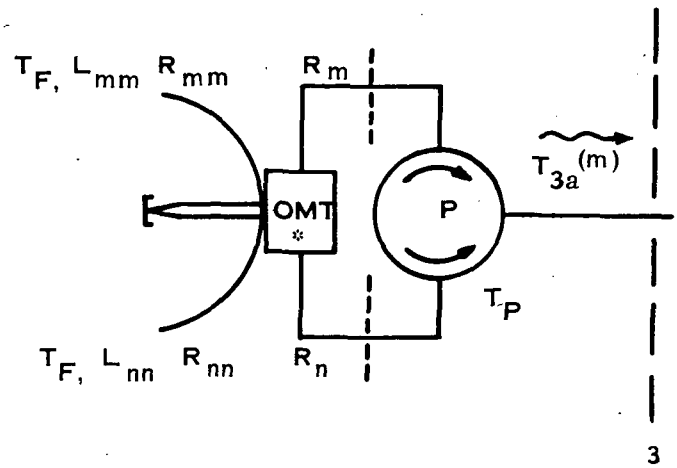


*Note: The OMT has a finite isolation between polarization modes. This coupled with the inherent antenna cross-polarization component will be treated as $C_{mn}$ (a pure ratio) where m is the desired polarization and n is the orthogonal polarization. Similarly, the OMT loss and antenna feed loss will be considered one loss with respect to each polarization.

Figure 4-4. Antenna Subassembly Block Diagram

Equation 22 ignores second order reflections and losses but does include for the sake of symmetry the cross-coupling terms though in practice they should be small. Equation 22 also defines a generator with a maximum available power due to the aforementioned sources and, in the subsequent developement of the analysis, will be used to complete the overall transfer function of the CCR.

The model in Figure 4-5 represents the switching subassembly containing reference planes 1, 2, 3, 4, 5.

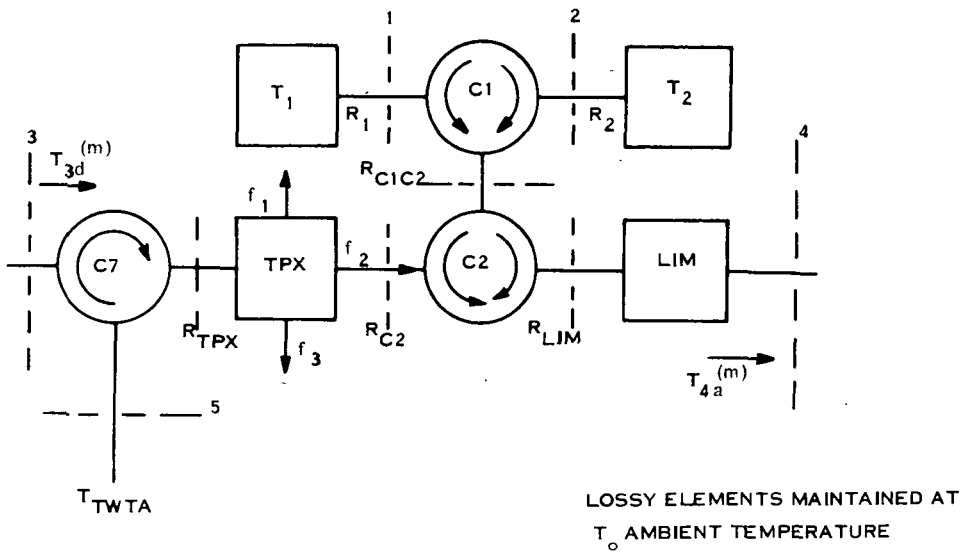


Figure 4-5. Switching Subassembly

In a manner similar to that used to generate $T_{3a}^{(m)}$, $T_{4a}^{(m)}$ is related to $T_{1d}$, $T_{2d}$, $T_{3d}$, $T_{5d}$ as follows:

With C2 → ANT and C1 → $T_1$

(A → B indicates energy passes from B to A)

and $T_{3d} = m\, T_{3a}$, $m = (1 - R_3)$ see Appendix A

$= T_{3a} (1 - R_3)$

and $T_{1d} = T_1 (1 - R_1)$

$T_{2d} = T_2 (1 - R_2)$

Then $T_{4a}^{(m)} = T_{3d}^{(m)} [L_{C7} L_{TPX} (1-R_{TPX}) L_{C2} (1-R_{C2}) L_{LIM} (1-R_{LIM})]$

$+ T_{1d} [L_{C1} L_{C2}^{2} (1-R_{C1C2}) L_{LIM} (1-R_{LIM}) R_{C2}]$

(cont)

$$+ T_{2d}\left[L_{C1}^{2} R_1 (1-R_{C1C2}) R_{C2} L_{C2}^{2} (1-R_{LIM}) L_{LIM}\right]$$

$$+ T_{TWTA}\left[(1-R_5) L_{C7}^{2} R_3 L_{TPX} (1-R_{TPX}) L_{C2} (1-R_{C2}) L_{LIM} (1-R_{LIM})\right]$$

$$+ T_o \Bigg[\Bigg\{\Big[\Big[(R_5 R_3 L_{C7}^{2} + R_3 L_{C7} + 1)(1-L_{C7})\Big](1-R_{TPX}) L_{TPX}$$

$$+ \left((1+R_{TPX} L_{TPX})(1-L_{TPX})\right)\Big](1-R_{C2})$$

$$+ L_{C2} R_{C2} (R_2 R_1 L_{C1}^{2} + R_1 L_{C1} + 1)(1-L_{C1})(1-R_{C1C2})\Bigg\} L_{C2}$$

$$+ (R_{C1C2} R_{C2} L_{C2}^{2} + R_{C2} L_{C2} + 1)(1-L_{C2})\Big](1-R_{LIM}) L_{LIM}$$

$$+ (1 + R_{LIM} L_{LIM})(1 - LIM)\Bigg] \qquad (23)$$

and for C2 → ANT, C1 → $T_2$

$$T_{4a}^{(m)} = T_{3d}\left[L_{C7} L_{TPX} (1-R_{TPX}) L_{C2} (1-R_{C2}) L_{LIM} (1-R_{LIM})\right]$$

$$+ T_{1d}\left[L_{C1}^{2} R_2 (1-R_{C1C2}) L_{C2}^{2} R_{C2} L_{LIM} (1-R_{LIM})\right]$$

$$+ T_{2d}\left[L_{C1} (1-R_{C1C2}) L_{C2}^{2} R_{C2} L_{LIM} (1-R_{LIM})\right]$$

$$+ T_{TWTA}\left[(1-R_5) L_{C7}^{2} R_3 L_{TPX} (1-R_{TPX}) L_{C2} (1-R_{C2}) \cdot L_{LIM} (1-R_{LIM})\right]$$

$$+ T_o \Bigg[\Bigg\{\Big[\Big[(R_5 R_3 L_{C7}^{2} + R_3 L_{C7} + 1)(1-L_{C7})\Big](1-R_{TPX}) \cdot L_{TPX} + (1 + R_{TPX} L_{TPX})(1-L_{TPX})\Big](1-R_{C2})$$

$$+ L_{C2} R_{C2} (R_1 R_2 L_{C1}^{2} + R_2 L_{C1} + 1)(1-L_{C1})(1-R_{C1C2})\Bigg\} L_{C2}$$

$$+ (R_{C1C2} R_{C2} L_{C2}^{2} + R_{C2} L_{C2} + 1)(1-L_{C2})\Big](1-R_{LIM}) L_{LIM}$$

$$+ (1 + R_{LIM} L_{LIM})(1-L_{LIM})\Bigg] \qquad (24)$$

for $C2 \rightarrow C1$, $C1 \rightarrow T_1$

$$T_{4a}^{(m)} = T_{1d}\left[L_{C1}\, L_{C2}\, (1 - R_{C1C2})\, L_{LIM}\, (1 - R_{LIM})\right]$$

$$+ T_{2d}\left[L_{C1}^{2}\, R_1\, L_{C2}\, (1-R_{C1C2})\, L_{LIM}\, (1-R_{LIM})\right]$$

$$+ T_{3d}\left[L_{C7}\, L_{TPX}\, (1-R_{TPX})\, L_{C2}^{2}\, (1-R_{C2})\, (R_{C1C2})\, L_{LIM}\, (1-R_{LIM})\right]$$

$$+ T_{TWTA}\left[L_{C7}^{2}\, (1-R_5)\, R_3\, L_{TPX}\, (1-R_{TPX})\, L_{C2}^{2} \cdot (1-R_{C2})\, R_{C1C2}\, L_{LIM}\, (1 - R_{LIM})\right]$$

$$+ T_o\Bigg[\Bigg\{\Bigg\{\Big[\Big[(R_5\, R_3\, L_{C7}^{2} + R_3\, L_{C7} + 1)\, (1-L_{C7})\Big]\, (1-R_{TPX})\, L_{TPX}$$

$$+ (1 + R_{TPX}\, L_{TPX})\, (1 - L_{TPX})\Big]\, (1-R_{C2})\, L_{C2}\, R_{C1C2}$$

$$+ (R_2\, R_1\, L_{C1}^{2} + R_1\, L_{C1} + 1)\, (1-L_{C1})\, (1-R_{C1C2})\Bigg\}\, L_{C2}$$

$$+ (R_{C1C2}\, R_{C2}\, L_{C2}^{2} + R_{C1C2}\, L_{C2} + 1)\, (1-L_{C2})\Big]\, (1-R_{LIM})\, L_{LIM}$$

$$+ (1-R_{LIM}\, L_{LIM})\, (1-L_{LIM})\Bigg] \qquad (25)$$

and finally, with $C2 \rightarrow C1$, $C1 \rightarrow T_2$

$$T_{4a}^{(m)} = T_{1d}\left[L_{C1}^{2}\, R_2\, L_{C2}\, (1-R_{C1C2})\, L_{LIM}\, (1-R_{LIM})\right]$$

$$+ T_{2d}\left[L_{C1}\, L_{C2}\, (1-R_{C1C2})\, L_{LIM}\, (1-R_{LIM})\right]$$

$$+ T_{3d}\left[L_{C7}\, L_{TPX}\, (1-R_{TPX})\, L_{C2}^{2}\, (1-R_{C2})\, R_{C1C2} \cdot L_{LIM}\, (1-R_{LIM})\right]$$

$$+ T_{TWTA}\Big[L_{C7}^{2}\, (1-R_5)\, R_3\, L_{TPX}\, (1-R_{TPX})\, L_{C2}^{2} \cdot (1-R_{C2})\, R_{C1C2}\, L_{LIM}\, (1-R_{LIM})\Big]$$

(cont)

$$+ T_o \Bigg[ \Bigg\{ \Bigg\{ \Big[ \Big[ (R_5 R_3 L_{C7}^2 + R_3 L_{C7} + 1)(1-L_{C7}) \Big] (1-R_{TPX}) \cdot L_{TPX} + (1+R_{TPX} L_{TPX})(1-L_{TPX}) \Big] (1-R_{C2}) L_{C2} R_{C1C2} + (R_1 R_2 L_{C1}^2 + R_2 L_{C1} + 1)(1-L_{C1})(1-R_{C1C2}) \Bigg\} L_{C2} + (R_{C1C2} R_{C2} L_{C2}^2 + R_{C1C2} L_{C2} + 1)(1-L_{C2}) \Big] (1-R_{LIM}) L_{LIM} + (1+R_{LIM} L_{LIM})(1-L_{LIM}) \Bigg] \quad (26)$$

Note: $R_{C1C2} R_2 = R_2 R_{C1C2}$

$R_{C1C2}$ exists but is inaccessible in the system. Its magnitude and phase are subject to change with the state of C1 and C2. Similarly, $(1-R_{C7})$ is not treated when considering $T_{3d}$ since it is treated as $(1-R_3)$. Also, $R_{LIM}$ and $R_{C2}$ are subject to change with the state of C1 and C2. These are second order effects. For justification of the terms involving $T_o$, see Appendix B.

The receiver has the following parameters:

- $B$ - Effective noise bandwidth
- $G_{AGC}$ - AGC amplifier gain
- $G \cdot G_{AGC}$ - Receiver power gain
- $K$ - Boltzmann's constant
- $\gamma$ - Detection constant
- $T_R$ - Effective receiver noise temperature referred to reference plane 4

Figure 4-6 represents a model of the composite CCR system. Recalling the following terms,

$T_{Ae}^{(m)}$ - Effective received antenna noise temperature, when the $m^{th}$ polarization is selected, incident on reference plane 4,

$T_{1e}$ - Effective reference temperature incident on reference plane 4 when reference temperature No. 1 is selected,

$T_{2e}$ - Effective reference temperature incident on reference plane 4 when reference temperature No. 2 is selected,

then,

$$T_{Ae}^{(m)} = T_{4a}^{(m)} (1-R_4), \quad C2 \rightarrow \text{Ant}, \; C1 \rightarrow T_1, \; T_2 \tag{27}$$

$$T_{1e} = T_{4a}^{(m)} (1-R_4), \quad C2 \rightarrow C1 \text{ and } C1 \rightarrow T_1 \tag{28}$$

$$T_{2e} = T_{4a}^{(m)} (1-R_4), \quad C2 \rightarrow C1 \text{ and } C1 \rightarrow T_2 \tag{29}$$

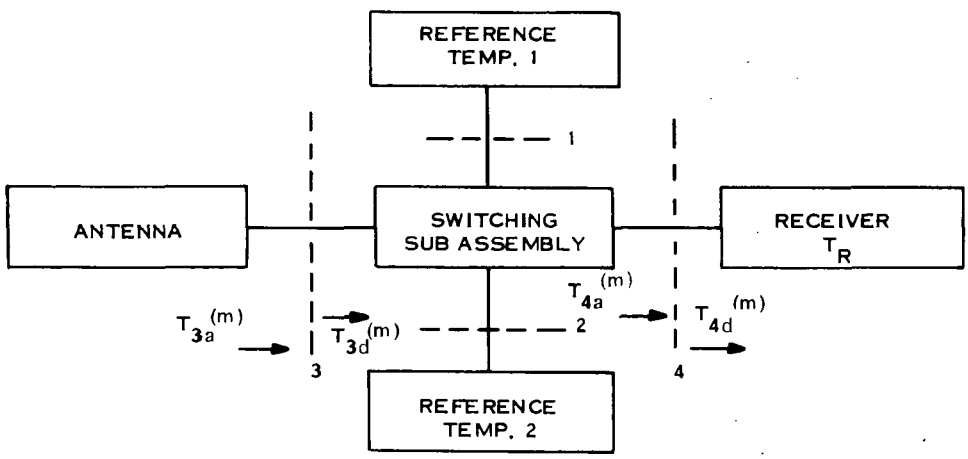


Figure 4-6. Composite CCR Model

By using equations 27, 28, 29 and the timing diagrams for the operational modes, the various CCR outputs will now be generated as a function of $T_{Ae}^{(m)}$, $T_{1e}$, and $T_{2e}$.

## 4.7 CCR OUTPUTS

Referring to Figures 2-2, 2-3 and 2-4 in Section 2, expressions will be found for the CCR outputs in the measurement mode, calibration mode, and baseline mode. Expressions for $G_{AGC}$, $V_{DATA}$, $T_{Ae}^{(m)}$, and $\xi$ (the normalized radiometer output) in terms of the constants (reference temperatures and other non-varying system constants) will also be derived.

Square Law Output

$$I(t) = -KBGG_{AGC}{}^{\gamma} \begin{cases} (T_R + T_{2e}) & 2K\tau \le t < 2K\tau + \tau/2 \\ \left(T_R + T_{Ae}^{(m)}\right) & 2K\tau + \tau/2 \le t < (2K+1)\,\tau \\ (T_R + T_{1e}) & (2K+1)\,\tau \le t < (2K+1)\,\tau + \tau/2 \\ \left(T_R + T_{Ae}^{(m)}\right) & (2K+1)\,\tau + \tau/2 \le t < (2K+2)\,\tau \end{cases} \quad K = 0,\ 1,\ 2 \ldots \tag{30}$$

Solving for $G_{AGC}$

$$I_{AGC} = -KBGG_{AGC}{}^{\gamma} \begin{cases} -(T_R + T_{2e}) & 2K\tau + \epsilon \le t < 2K\tau + \tau/2 \\ (T_R + T_{1e}) & (2K+1)\,\tau + \epsilon \le t < (2K+1)\,\tau + \tau/2 \\ 0 & \text{Elsewhere} \end{cases} \quad K = 0,\ 1,\ 2 \ldots \tag{31}$$

For AGC steady state solution

$$-\frac{1}{C_A}\int_0^{N\tau}(I_{AR}+I_{AGC})\,dt=\langle V_{AGC}\rangle \tag{32}$$

N, the number of operating periods $>2$

Where $\langle V_{AGC}\rangle$ and $I_{AR}$ are assumed negative and $\langle V_{AGC}\rangle$ is the steady state AGC voltage

$$\int_0^{N\tau}(I_{AR}+I_{AGC})\,dt=-\langle V_{AGC}\rangle C_A \tag{33}$$

For the steady state condition to occur in the AGC loop, the time average of $I_{AGC}$ (denoted $\langle I_{AGC}\rangle$ must equal $-I_{AR}$. Thus,

$$I_{AR}+\langle I_{AGC}\rangle = 0 \tag{34}$$

and

$$\langle I_{AGC}\rangle = \frac{(\tau/2-\epsilon)}{2\tau}\,KBGG_{AGC}\gamma\,(T_{1e}-T_{2e}) \tag{35}$$

From (34), (35) we may compute $G_{AGC}$

$$G_{AGC}=\frac{-I_{AR}\,2\tau}{KBG\gamma\,(T_{1e}-T_{2e})\,(\tau/2-\epsilon)} \tag{36}$$

Letting $a=\dfrac{-2\tau\,I_{AR}}{(\tau/2-\epsilon)}$ (37)

$$G_{AGC}=\frac{a}{KBG\gamma\,(T_{1e}-T_{2e})} \tag{38}$$

for all modes of radiometer operation.

Computing Baseline Calibration

$$I(t) = -KBGG_{AGC}{}^{\gamma} \begin{cases} (T_R + T_{2e}) \\ (T_R + T_{1e}) \end{cases} \begin{matrix} 2K\tau \le t < (2K+1)\tau \\ (2K+1)\tau \le t < (2K+2)\tau \end{matrix} \qquad (39)$$

$$K = 0, 1, 2 \ldots$$

$$I_{Data} = -KBGG_{AGC}{}^{\gamma} \begin{cases} -(T_R + T_{2e}) \\ +(T_R + T_{2e}) \\ +(T_R + T_{1e}) \\ -(T_R + T_{1e}) \end{cases} \begin{matrix} 2K\tau + \epsilon \le t < 2K\tau + \tau/2 \\ 2K\tau + \tau/2 + \epsilon \le t < (2K+1)\tau \\ (2K+1)\tau + \epsilon \le t < (2K+1)\tau + \tau/2 \\ (2K+1)\tau + \tau/2 + \epsilon \le t < (2K+2)\tau \end{matrix} \qquad (40)$$

$$K = 0, 1, 2 \ldots$$

$$V_{DATA} = \frac{-1}{C_D} \int_0^{N\tau} (I_{DATA} + I_{DR})\, dt$$

$$V_{DATA} = \frac{-1}{C_D} \int_0^{N\tau} \left(-\frac{KBG}{4} G_{AGC}{}^{\gamma}(0) + I_{DR}\right) dt$$

$$V_{DATA} = \frac{-2N(\tau/2 - \epsilon) I_{DR}}{C_D}, \quad (I_{DR} \text{ negative}) \qquad (41)$$

The result is a baseline voltage produced by adding and subtracting identical temperatures.

$$V_B = \frac{-2N\,(\tau/2 - \epsilon)}{C_D}\ I_{DR} \tag{42}$$

Computing Normal Calibration

$$I(t) = -\,KBGG_{AGC}\gamma \begin{cases} -(T_R+T_{2e}) & 2K\tau+\epsilon \le t < 2K\tau+\tau/2 \\ -(T_R+T_{2e}) & 2K\tau+\tau/2+\epsilon \le t < (2K+1)\,\tau \\ +(T_R+T_{1e}) & (2K+1)\,\tau+\epsilon \le t < (2K+1)\,\tau+\tau/2 \\ +(T_R+T_{1e}) & (2K+1)\tau+\tau/2+\epsilon \le t < (2K+2)\,\tau \end{cases} \tag{43}$$

$$K = 0,\ 1,\ 2 \ldots$$

$$I_{DATA} = -\,KBGG_{AGC}\gamma \begin{cases} -(T_R+T_{2e}) & 2K\tau \le t < (2K+1)\,\tau \\ (T_R+T_{1e}) & (2K+1)\,\tau \le t < (2K+2)\,\tau \end{cases} \tag{44}$$

$$V_{CAL} = \frac{-1}{C_D} \int_0^{M\tau} (I_{DATA} + I_{DR})\,dt$$

M, the number of calibration periods, $> 2$

$$V_{CAL} = \frac{M}{N}\,V_B - \frac{1}{C_D} \int_0^{M\tau} I_{DATA}\,dt$$

$$V_{CAL} = \frac{M}{N}\,V_B + \frac{KBGG_{AGC}\,\gamma\,M\,(T_{1e} - T_{2e})\,(\tau/2 - \epsilon)}{C_D} \tag{45}$$

using (36) and (45)

$$V_{CAL} = \frac{M}{N}\,V_B - \frac{2M\tau\,I_{AR}}{C_D}\ , \quad (I_{AR} < 0) \tag{46}$$

Computation of the Measurement Mode

$$I(t) = -KBGG_{AGC}\gamma \begin{cases} +(T_R+T_{2e}) & 2K\tau \le t < 2K\tau + \tau/2 \\ +(T_R+T_{Ae}^{(m)}) & 2K\tau + \tau/2 \le t < (2K+1)\tau \\ +(T_R+T_{1e}) & (2K+1)\tau \le t < (2K+1)\tau + \tau/2 \\ +(T_R+T_{Ae}^{(m)}) & (2K+1)\tau + \tau/2 \le t < (2K+2)\tau \end{cases} \quad (30)$$

$$K = 0,\ 1,\ 2 \ldots$$

$$I_{DATA} = -KBGG_{AGC}\gamma \begin{cases} +(T_R+T_{2e}) & 2K\tau+\epsilon \le t < 2K\tau + \tau/2 \\ -(T_R+T_{Ae}^{(m)}) & 2K\tau + \tau/2 + \epsilon \le t < (2K+1)\tau \\ +(T_R+T_{1e}) & (2K+1)\tau + \epsilon \le t < (2K+1)\tau + \tau/2 \\ -(T_R+T_{Ae}^{(m)}) & (2K+1)\tau + \tau/2 + \epsilon \le t < (2K+2)\tau \end{cases} \quad (47)$$

$$K = 0,\ 1,\ 2 \ldots$$

for polarization choice m

$$V_{DATA} = V_B - \frac{1}{C_D} \int_0^{N\tau} I_{DATA}\, dt$$

N, the number of operational periods, > 2

using (47)

$$V_{DATA} = V_B + \frac{KBGG_{AGC}\gamma}{2C_D} N\,(T_{1e}+T_{2e} - 2T_{Ae}^{(m)})\,(\tau/2 - \epsilon)$$

and using (36)

$$V_{DATA}^{(m)} = V_B - \frac{N\tau\, I_{AR}\,(T_{1e} + T_{2e} - 2\,T_{Ae}^{(m)})}{C_D\,(T_{1e} - T_{2e})} \quad (48)$$

Solving (46) for $I_{AR}$ and substituting it into (48)

$$V_{DATA} = V_B + \left[\frac{N}{M} V_{CAL} - V_B\right] \frac{\left[T_{1e} + T_{2e} - 2T_{Ae}^{(m)}\right]}{2\,(T_{1e} - T_{2e})} \tag{49}$$

Rearranging (49) to solve for $T_{Ae}^{(m)}$ or $\xi$ (normalized radiometer output)

$$T_{Ae}^{(m)} = \frac{1}{2}\left[\left[T_{1e}+T_{2e}\right] - \frac{2\left[V_{DATA} - V_B\right]}{\left[\frac{N}{M} V_{CAL} - V_B\right]}\left[T_{1e} - T_{2e}\right]\right] \tag{50a}$$

or,

$$\xi = \frac{(T_{1e}+T_{2e} - 2T_{Ae}^{(m)})}{2\,(T_{1e} - T_{2e})} = \frac{(V_{DATA} - V_B)}{(\frac{N}{M} V_{CAL} - V_B)} \tag{50b}$$

When $V_{DATA}^{(m)} = V_B$, the baseline represents the equivalent Dicke reference temperature, $\left[\frac{T_{1e} - T_{2e}}{2}\right]$.

## 4.8 MINIMUM DETECTABLE SIGNAL

The general expression[11] for the RMS fluctuations of a simple radiometer using a simple integrator (one time constant, $\tau_i$ = RC), bandwidth B, and square law detector is given by

$$\Delta T = \frac{T}{\sqrt{2B\tau_i}} \tag{51}$$

where T is the sum of the unknown temperature $T_X$, at the input to the radiometer and the effective receiver temperature, $T_R$.

Due to the switching nature of the CCR,

$$T = \begin{cases} (T_{1e} + T_R) & 2K\tau \le t < 2K\tau + \tau/2 \\ (T_{Ae}^{(m)} + T_R) & 2K\tau + \tau/2 \le t < (2K+1)\tau \\ (T_{2e} + T_R) & (2K+1)\tau \le t < (2K+1)\tau + \tau/2 \\ (T_{Ae}^{(m)} + T_R) & (2K+1)\tau + \tau/2 \le t < (2K+2)\tau \end{cases} \quad (52)$$

The following, then, are expressions for the fluctuations of the radiometer depending on the position of the Dicke and $\Delta T$ switches.

Reference 1 selected: $$\Delta T_1 = \frac{T_{1e} + T_R}{\sqrt{B\tau_i/2}} \quad (53)$$

Reference 2 selected: $$\Delta T_2 = \frac{T_{2e} + T_R}{\sqrt{B\tau_i/2}} \quad (54)$$

Antenna selected: $$\Delta T_A = \frac{T_{Ae}^{(m)} + T_R}{\sqrt{B\tau_i/2}} \quad (55)$$

Both the AGC and DATA outputs are formed from different linear combinations of these four uncorrelated temperature measurements during a measurement period. The RMS value of the fluctuation of the combination is calculated by the quadratic addition[12] of the RMS values of the fluctuations of the respective temperatures. The AGC channel has a $\tau_i = \tau_{AGC}$ and the DATA channel has a $\tau_i = \tau_{DATA}$. From the expression for $I_{AGC}$, (31) it is evident that $I_{AGC}$ is directly proportional to $(T_{1e} - T_{2e})$. Thus

$$\frac{\Delta I_{AGC}}{I_{AGC}} = \Delta \frac{(T_{1e} - T_{2e})}{T_{1e} - T_{2e}}$$

$$= \frac{\sqrt{(T_{1e} + T_R)^2 + (T_{2e} + T_R)^2}}{(T_{1e} - T_{2e})\sqrt{B\tau_{AGC}/2}} \qquad (56)$$

Note that (56) does not include contributions from the antenna, an improvement over Hach's radiometer[15] obtained by adjusting Hach's parameter, $\alpha$, the phasing between the Dicke and $\Delta T$ switch. Adjusting for zero phase delay and blanking the switching transients after detection resulted in this improvement.

Similarly,

$$\frac{\Delta I_{DATA}}{I_{DATA}} = \frac{\sqrt{(T_{1e} + T_R)^2 + (T_{2e} + T_R)^2 + 2\,(T_{Ae}^{(m)} + T_R)^2}}{(T_{1e} + T_{2e} - 2T_{Ae}^{(m)})\sqrt{B\tau_{DATA}/2}} \qquad (57)$$

Two methods will be used to compute the fluctuation of the radiometer output.

Direct Method

Consider the ratio of $V_{DATA}/V_{AGC}$ or $I_{DATA}/I_{AGC}$. Note that these ratios are equivalent to $\xi$, the normalized radiometer output (see equations 16b, 50b). Assuming the fluctuations in (56) and (57) to be small compared to 1, and that $I_{DATA}$ and $I_{AGC}$ are uncorrelated, then the normalized fluctuation is

$$\frac{\Delta T}{(T_{1e} - T_{2e})} = \Delta (I_{DATA}/I_{AGC}) = (I_{DATA}/I_{AGC})\sqrt{\left(\frac{\Delta I_{DATA}}{I_{DATA}}\right)^2 + \left(\frac{\Delta I_{AGC}}{I_{AGC}}\right)^2} \qquad (58)$$

Substituting (31), (47), (56) and (57) into (58), and multiplying by $(T_{1e} - T_{2e})$ (normalizing factor) to compute the actual fluctuation $\Delta T$

$$\Delta T = \sqrt{\frac{(T_{1e} + T_R)^2 + (T_{2e} + T_R)^2 + 2\,(T_{Ae}{}^{m} + T_R)^2}{B\tau_{DATA}/2} + \frac{(T_{1e} + T_{2e} - 2T_{Ae}{}^{(m)})^2\left((T_{1e} + T_R)^2 + (T_{2e} + T_R)^2\right)}{(T_{1e} - T_{2e})^2\, B\tau_{AGC}/2}} \qquad (59)$$

combining terms,

$$\Delta T = \sqrt{\frac{\left[(T_{1e} + T_R)^2 + (T_{2e} + T_R)^2 + 2(T_{Ae}{}^{(m)} + T_R)^2\right] + \frac{\tau_{DATA}}{\tau_{AGC}}\left[\frac{(T_{1e} + T_{2e} - 2T_{Ae}{}^{(m)})}{(T_{1e} - T_{2e})}\right]^2\left[(T_{1e} + T_R)^2 + (T_{2e} + T_R)^2\right]}{\sqrt{2B\tau_{DATA}}}}$$

and then rearranging them,

$$\Delta T = \sqrt{\frac{\left[1 + \frac{\tau_{DATA}}{\tau_{AGC}}\,\frac{(T_{1e} + T_{2e} - 2T_{Ae}{}^{(m)})^2}{(T_{1e} - T_{2e})^2}\right]\left[(T_{1e} + T_R)^2 + (T_{2e} + T_R)^2\right] + 2\,(T_{Ae}{}^{(m)} + T_R)^2}{\sqrt{2B\tau_{DATA}}}} \qquad (60)$$

AGC Method

The second method of expressing the minimum detectable signal is to let the AGC current, $I_{AGC}$, be held to a constant value $I_o$ and let all fluctuations in $\Delta\,(T_{1e} - T_{2e})$ result in a $\Delta\,G_o$, common to both the DATA and AGC channels.

$$\text{Hence, } \frac{\Delta G_o}{G_o} = \frac{\Delta\,(T_{1e} - T_{2e})}{(T_{1e} - T_{2e})} = \frac{\Delta\, I_{AGC}}{I_{AGC}} \qquad (61)$$

The gain fluctuation now results in an additional data fluctuation such that the total RMS fluctuation in (47) is

$$\frac{\Delta I_{DATA}}{I_{DATA}} = \sqrt{\left(\frac{\Delta G_o}{G_o}\right)^2 + \left[\frac{\Delta\,(T_{1e} + T_{2e} - 2T_{Ae}{}^{(m)})}{(T_{1e} + T_{2e} - 2T_{Ae}{}^{(m)})}\right]^2} \qquad (62)$$

Since the reference temperature fluctuations act upon the data path after being smoothed by the AGC loop, $\tau_i$ becomes for (61), the sum of $\tau_{AGC}$ and $\tau_{DATA}$:

$$\tau_i = \tau_{DATA} + \tau_{AGC} \tag{63}$$

Hence, from (56), (61) and (63)

$$\frac{\Delta G_o}{G_o} = \frac{\sqrt{(T_{1e} + T_R)^2 + (T_{2e} + T_R)^2}}{(T_{1e} - T_{2e})\sqrt{B(\tau_{AGC} + \tau_{DATA})/2}} \tag{64}$$

Substituting (57) and (64) into (62) directly yields an expression of radiometer output fluctuation.

$$\frac{\Delta I_{DATA}}{I_{DATA}} = \sqrt{\frac{(T_{1e} + T_R)^2 + (T_{2e} + T_R)^2}{(T_{1e} - T_{2e})^2 B(\tau_{AGC} + \tau_{DATA})/2} + \frac{(T_{1e} + T_R)^2 + (T_{2e} + T_R)^2 + 2(T_{Ae}^{(m)} + T_R)^2}{(T_{1e} + T_{2e} - 2T_{Ae}^{(m)})^2 B\tau_{DATA}/2}} \tag{65}$$

Rearranging the terms and solving for $\Delta T$,

$$\Delta T = \frac{\sqrt{\left[1 + \frac{1}{1 + \tau_{AGC}/\tau_{DATA}} \frac{(T_{1e} + T_{2e} - 2T_{Ae}^{(m)})^2}{(T_{1e} - T_{2e})^2}\right]\left[(T_{1e} + T_R)^2 + (T_{2e} + T_R)^2\right] + 2(T_{Ae}^{(m)} + T_R)^2}}{\sqrt{2B\tau_{DATA}}} \tag{66}$$

Again, equation 66 shows the improvement over Hach[15]. Equations 60 and 66 show that not only does the DATA integration time constant affect the minimum detectable signal but also the ratio $\tau_{AGC}/\tau_{DATA}$. Note also that in the limit as $\tau_{AGC}$ approaches zero for the direct case, $\Delta T$ has an unbounded upper limit. This may be explained by remembering that it was arbitrarily assumed that $I_{DATA}$ and $I_{AGC}$ were uncorrelated. This is not true for small values of $\tau_{AGC}/\tau_{DATA}$. However, for the AGC method, $\Delta T$ is bounded. In the limit, then, as $\tau_{AGC}/\tau_{DATA}$ becomes very large, $\Delta T$, approaches that of the Dicke radiometer:

## 4.9 SENSITIVITY

From the results of Section 4.8 it is apparent that $\Delta T\sqrt{B\tau_{DATA}}$ is a

good measure of the sensitivity (i.e., Figure of Merit) of radiometers. It allows comparison of different radiometers without correcting for their different bandwidths and data integration time constants. Tomiyasu[16] has proposed a similar Figure of Merit, $\frac{B}{NF}$

where B = Bandwidth

NF = Noise Figure

related to $\Delta T$ by the relationship

$$\Delta T \sqrt{\tau B} = K(NF)\, T_o$$

or

$$\frac{B}{NF} = \frac{K\, T_o^{\,2}}{\Delta T^2\, \tau_{DATA}} \tag{67}$$

which is useful when working with measured performance data, but less convenient to use for analysis since $\Delta T$ embodies both B and NF.

Figure 4-7 is a plot of the expression $\Delta T \sqrt{B\tau_{DATA}}$ for both the Direct and the AGC methods of computing sensitivity. Either method, as can be seen from this figure, gives a good estimate of the sensitivity of the CCR for $\tau_{AGC}/\tau_{AGC} > 1$ and the bounded behavior of the AGC method is also clearly illustrated for $0 \le T_{Ae}^{(m)} \le \frac{(T_{1e} + T_{2e})}{2}$. By choosing $\tau_{AGC}/\tau_{DATA} \approx 100$ for $0 \le T_{Ae}^{(m)} \le \frac{T_{1e} + T_{2e}}{2}$ one obtains the most symmetrical curve and a minimum variation in sensitivity. However, one must exercise caution using the sensitivity expression for radiometer design. It would first appear that reducing $\tau_{DATA}$ to zero would yield a perfect system. However, $\Delta T$

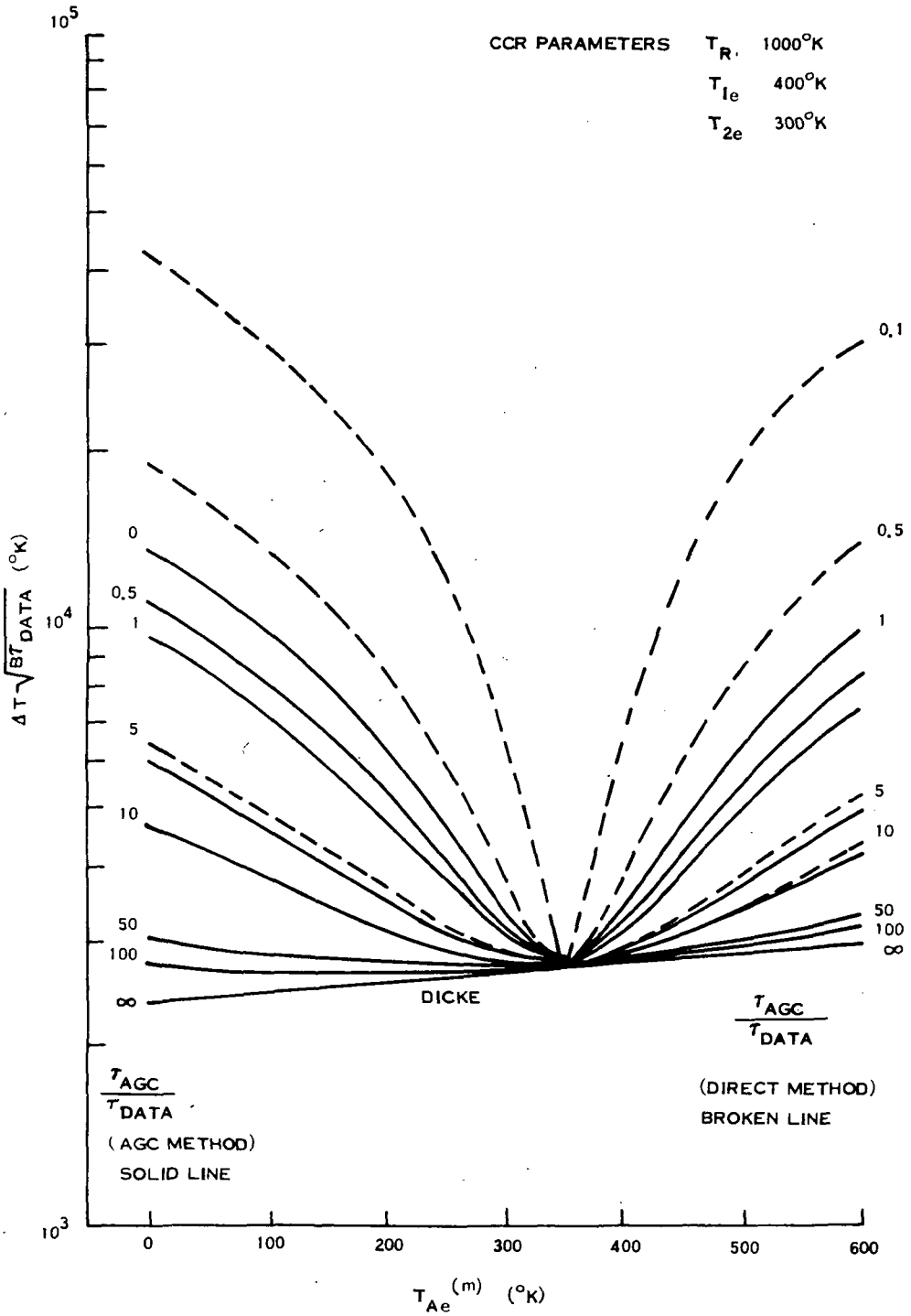


Figure 4-7. CCR Sensitivity vs. Antenna Temperature

embodies $\tau_{DATA}$ as well. Therefore, for design purposes equation 66, expressing the minimum detectable signal (MDS), is a better design tool. One should choose $\tau_{AGC}/\tau_{DATA}$ for the desired MDS and choose $\tau_{DATA}$ compatible with desired instrument response time.

4.10 ACCURACY

The expressions for the minimum detectable signal, sensitivity, and $V_{DATA}$ (or $I_{DATA}$) contain $T_{Ae}^{(m)}$, $T_{1e}$, $T_{2e}$. These terms, expressed by equations 27, 28, and 29 respectively, are very complex and tedious to evaluate. What is immediately apparent when analyzing the expressions for $T_{4a}^{(m)}$ (equations 23-26) are the terms involving the two reference temperatures, the antenna, the TWTA, and the contribution of ambient temperatures by component losses. Hach[17] assumed a low loss, low VSWR system and simplified these expressions. However, he noted that for higher insertion losses, corrections would become indispensable for accurate measurements. His correction dealt only with the loss factor in the antenna system and the added noise contributed by it.

The following analysis will assess the magnitude of error or bias introduced by the losses and VSWR's. An expression representative of MDS, sensitivity and $V_{DATA}$ will be analyzed. Equation 50b, repeated here for convenience, will be used for the analysis.

$$\xi = \frac{V_{DATA} - V_B}{\frac{N}{M} V_{CAL} - V_B} = \frac{T_{1e} + T_{2e} - 2\,T_{Ae}^{(m)}}{2\,(T_{1e} - T_{2e})} \qquad (50b)$$

Only one approximation will be made. It will be assumed that $R_1$ and $R_2$ are of equal magnitude, R, and that they are stable both long and short term.

Substituting equations 23 through 29 into 50b, the following expressions are generated:

$$(T_{1e}+T_{2e}) = (T_1+T_2)\,(1-R)\,[\,(1+L_{C1}R)\,L_{C1}\,L_{C2}\,(1-R_{C1C2})\,L_{LIM}\,(1-R_{LIM})]$$
$$+ 2T_{3a}\,(1-R_3)\,[L_{C7}\,L_{TPX}\,(1-R_{TPX})\,L_{C2}^{\,2}\,(1-R_{C2})\,R_{C1C2}\,L_{LIM}\cdot (1-R_{LIM})\,]$$
$$+ 2T_o\Big[\Big\{\Big\{\Big\{\Big[\big[(R_5R_3L_{C7}^{\,2}+R_3L_{C7}+1)\,(1-L_{C7})\big]\,(1-R_{TPX})\,L_{TPX}$$
$$+ (1+R_{TPX}\,L_{TPX})\,(1-L_{TPX})\Big]\,(1-R_{C2})\,L_{C2}\,R_{C1C2}$$
$$+ (R^2\,L_{C1}^{\,2}+RL_{C1}+1)\,(1-L_{C1})\,(1-R_{C1C2})\Big\}\,L_{C2}$$
$$+ (R_{C1C2}\,R_{C2}\,L_{C2}^{\,2}+R_{C1C2}\,L_{C2}+1)\,(1-L_{C2})\Big]\,(1-R_{LIM})\,L_{LIM}$$
$$+ (1+R_{LIM}\,L_{LIM})\,(1-L_{LIM})\Big]$$
$$+ 2T_{TWTA}\Big[L_{C7}^{\,2}\,(1-R_5)\,R_3L_{TPX}(1-R_{TPX})\,L_{C2}^{\,2}\,(1-R_{C2})\,R_{C1C2}\cdot L_{LIM}\,(1-R_{LIM})\Big] \qquad (68)$$

$$(T_{1e}-T_{2e}) = (T_1-T_2)\,(1-L_{C1}R)\,L_{C1}\,(1-R)\,L_{C2}\,(1-R_{C1C2})\,L_{LIM}\cdot (1-R_{LIM}) \qquad (69)$$

$$2T_{Ae}^{(m)} = 2T_{3a}\,(1-R_3)\,[L_{C7}\,L_{TPX}\,(1-R_{TPX})\,L_{C2}\,(1-R_{C2})\,L_{LIM}\cdot (1-R_{LIM})] \qquad \text{(cont)}$$

$$+ (T_1+T_2)(1-R)\left[(1+R\,L_{C1})\,L_{C1}(1-R_{C1C2})\cdot L_{C2}^{\,2}\,R_{C2}\,L_{LIM}(1-R_{LIM})\right]$$

$$+ 2\,T_{TWTA}\left[(1-R_5)\,L_{C7}^{\,2}\,R_3\,L_{TPX}(1-R_{TPX})\cdot L_{C2}(1-R_{C2})\,L_{LIM}(1-R_{LIM})\right]$$

$$+ 2T_o\left[\left\{\left\{\left[(R_5R_3L_{C7}^{\,2}+R_3L_{C7}+1)(1-L_{C7})\right](1-R_{TPX})\,L_{TPX}\right.\right.\right.$$

$$\left.\left.\left.+(1+R_{TPX}\,L_{TPX})(1-L_{TPX})\right](1-R_{C2})\right.\right.$$

$$\left.+L_{C2}\,R_{C2}\,(R^2L_{C1}^{\,2}+RL_{C1}+1)(1-L_{C1})(1-R_{C1C2})\right\}L_{C2}$$

$$+(R_{C1C2}\,R_{C2}\,L_{C2}^{\,2}+R_{C2}\,L_{C2}+1)(1-L_{C2})\Big](1-R_{LIM})\,L_{LIM}$$

$$+(1+R_{LIM}\,L_{LIM})(1-L_{LIM})\Big] \qquad (70)$$

Combining (68) and (70),

$$T_{1e}+T_{2e}-2T_{Ae}^{(m)} = (T_1+T_2)(1-R)(1+RL_{C1})\,L_{C1}(1-R_{C1C2})\cdot L_{C2}\,L_{LIM}(1-R_{LIM})(1-L_{C2}R_{C2})$$

$$-2T_{3a}(1-R_3)\,L_{C7}\,L_{TPX}(1-R_{TPX})\,L_{C2}\cdot(1-R_{C2})\,L_{LIM}(1-R_{LIM})(1-L_{C2}\,R_{C1C2})$$

$$-2T_{TWTA}(1-R_5)\,L_{C7}^{\,2}\,R_3\,L_{TPX}(1-R_{TPX})\cdot L_{C2}(1-R_{C2})\,L_{LIM}(1-R_{LIM})(1-L_{C2}\,R_{C1C2})$$

$$-2T_o\left[\left\{\left\{\left[(R_5R_3L_{C7}^{\,2}+R_3\,L_{C7}+1)(1-L_{C7})\right]\cdot(1-R_{TPX})\,L_{TPX}\right.\right.\right.$$

(cont)

$$+ (1+R_{TPX}\,L_{TPX})\,(1-L_{TPX})\Big]\,(1-R_{C2})\Big\}\cdot$$

$$+ (R^2\,L_{C1}^{\,2} + RL_{C1} + 1)\,(1 - L_{C1}\,(1 - R_{C1C2})\cdot$$

$$L_{C2}\,(1 - L_{C2}\,R_{C1C2})$$

$$+ \Big[(R_{C1C2}\,R_{C2}\,L_{C2}^{\,2} + R_{C1C2}\,L_{C2} + 1)$$

$$- (R_{C1C2}\,R_{C2}\,L_{C2}^{\,2} + R_{C2}\,L_{C2} + 1)\Big]\,(1-L_{C2})\Big]\cdot$$

$$(1-R_{LIM})\,L_{LIM} + (1+R_{LIM}\,L_{LIM})\,(1-L_{LIM})\Big] \tag{71}$$

Note that in the final expression for $\xi$ (not explicitly written, $\xi = \frac{\text{Eqn 71}}{\text{Eqn 69}}$) the term $(1 - R_4)$ does not appear. Note also that terms of the form, $(1 - LR)$, $(1 - L)$, $(1 - R)$, appear in equations 69 and 71. Expressing $\xi$ in the following manner should clarify this point.

$$\xi = [K_1\,(T_1 + T_2)\,(1 - L_{C2}\,R_{C2}) + (K_2 T_{3a} + K_3\,T_{TWTA})\cdot$$

$$(1 - L_{C2}\,R_{C1C2}) + K_4\,T_o] \div [K_5 (T_1 - T_2)\,(1 - L_{C1}\,R)] \tag{72}$$

where the $K_i$ are combined reflection and loss constants found in equations 69 and 71.

The importance of equation 72 becomes apparent when compared with equation 21. In actual practice, while the reflection coefficient at the input of the receiver (if constant) does not enter into consideration, all losses before the receiver input do enter into consideration, and, if the reflection coefficients are not small, many terms exist which are significant and cannot be dropped. In all cases, however, a scale factor $(1 - L_{C1}\,R)$, related

to the temperature references, appears in equation 50b and must always be considered.

Figure 4-8 illustrates the magnitude of the antenna temperature correction in degrees Kelvin which must be added (subtracted) to (from) the antenna temperature. (R, L, LR ) are expressed in dB.

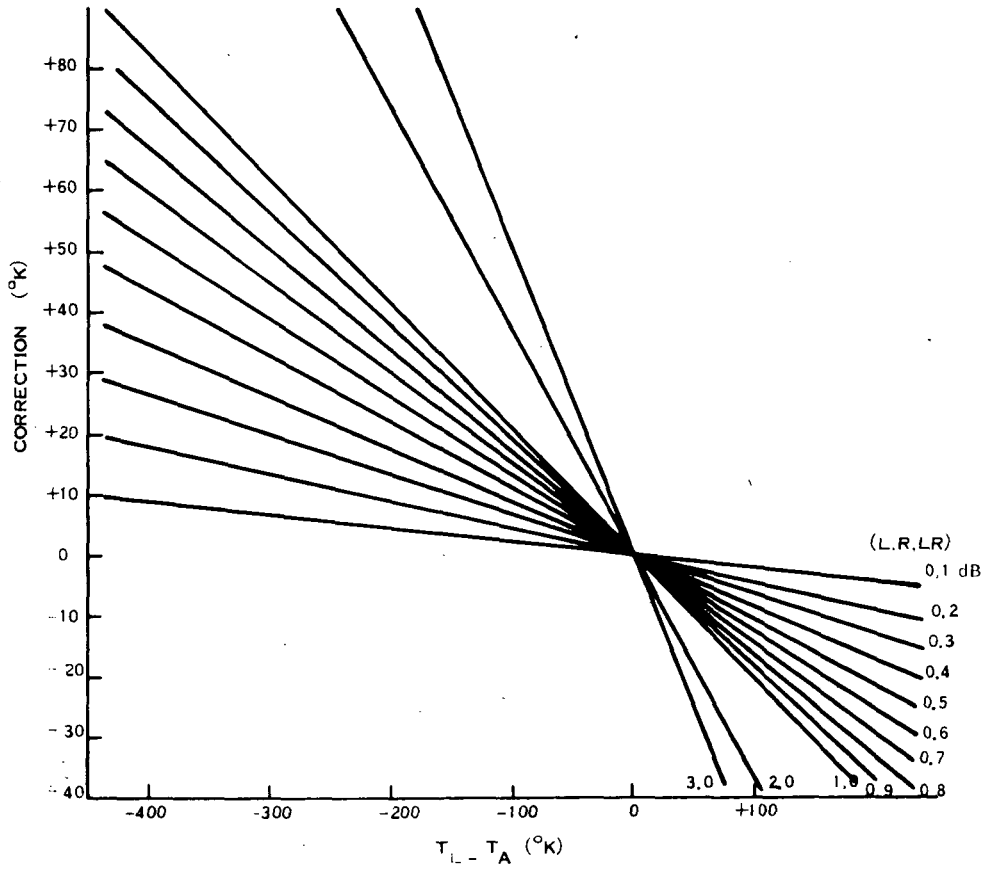


Figure 4-8. Radiometric Temperature Correction Factors

## SECTION 5

## APPLICATION OF THE GENERAL SOLUTION TO THE AAFE RADSCAT

The predicted and experimental values of minimum detectable signal (MDS), sensitivity, and accuracy of the AAFE RADSCAT were computed using the foregoing analysis. Key system parameters used in the analysis are listed in Table 5-1. The results are summarized in Table 5-2. Figures 5-1, 5-2 and 5-3 are plots of the data in Table 5-2.

Table 5-1. RADSCAT Radiometer System Parameters

| | | |
|---|---|---|
| $\frac{\tau_{AGC}}{\tau_{DATA}}^{*}$ | = | 2, 10 |
| $T_R$ | = | $1500^{o}K$ |
| $T_{1e}$ | = | $400^{o}K$ |
| $T_{2e}$ | = | $311^{o}K$ |
| $T_{TWTA}$ | = | $380^{o}K$ |
| $T_o$ | = | $311^{o}K$ |
| $T_A^{(n)}$ | = | $13^{o}K$ |
| $T_F$ | = | $298^{o}K$ |
| $T_P$ | = | $298^{o}K$ |
| B | = | 200 MHz |
| $\tau_{AGC}^{*}$ | = | 0.10 seconds, 0.5 seconds |
| $\tau_{DATA}$ | = | 0.05 seconds |
| N | = | 128 |
| M | = | 100 |
| $\tau$ | = | 0.001 seconds |

*The system was modified during August 1972 and $\tau_{AGC}$ was changed from 0.1 sec to 0.5 sec.

Table 5-2. RADSCAT Performance

| | $T_A^{(m)}$ | $T_{Ae}^{(m)*}$ | $\Delta T\sqrt{B\,\tau_{DATA}}$ | | $\Delta T$ | | $\xi$ |
|---|---|---|---|---|---|---|---|
| | | | $\tau_{AGC}/\tau_{DATA} = 10$ | $\tau_{AGC}/\tau_{DATA} = 2$ | $\tau_{AGC}/\tau_{DATA} = 10$ | $\tau_{AGC}/\tau_{DATA} = 2$ | |
| THEORY | 0 | 128.8 | 5335 | 8475 | 1.20 | 1.89 | 2.55 |
| | 50 | 158.1 | 4972 | 7588 | 1.11 | 1.70 | 2.22 |
| | 100 | 187.4 | 4640 | 6735 | 1.04 | 1.51 | 1.89 |
| | 150 | 216.7 | 4097 | 5927 | 0.97 | 1.33 | 1.56 |
| | 200 | 246.0 | 3903 | 5186 | 0.92 | 1.16 | 1.23 |
| | 250 | 275.3 | 3753 | 4545 | 0.88 | 1.02 | 0.90 |
| | 300 | 304.6 | 3772 | 4051 | 0.85 | 0.91 | 0.57 |
| | 350 | 333.9 | 3710 | 3763 | 0.83 | 0.84 | 0.24 |
| | 400 | 363.2 | 3719 | 3729 | 0.83 | 0.83 | -0.09 |
| | 450 | 392.5 | 3806 | 3955 | 0.85 | 0.88 | -0.42 |
| | 500 | 421.8 | 3958 | 4402 | 0.89 | 0.98 | -0.74 |

*$T_{Ae}^{(m)} = 128.8 + 0.586\ T_A$

Table 5-2. RADSCAT Performance (Cont)

| | $T_A$ | $\tau_{AGC}/\tau_{DATA}$ | $\Delta T$ | $\xi$ | $\Delta T\sqrt{B\tau_{DATA}}$ |
|---|---|---|---|---|---|
| EXPERIMENTAL RESULTS | 307 | 2 | 1.84 | Invalid | 5818 |
| | 43.7 | 2 | 3.83 | Data | 12112 |
| | 316 | 2 | 1.85 | ↓ | 5850 |
| | 109.7 | 2 | 2.54 | ↓ | 8032 |
| Table* Mountain Antenna Tests | 117 | 2 | 2.52 | ↓ | 7969 |
| | 347 | 2 | 1.62 | ↓ | 5123 |
| | 65.8 | 2 | 2.87 | ↓ | 9076 |
| | 80.9 | 2 | 2.89 | ↓ | 9139 |
| | 72.3 | 2 | 3.87 | ↓ | 12238 |
| | 66 | 2 | 3.00 | ↓ | 9487 |
| Laboratory Tests at GE | 77 | 10 | 1.73 | 2.09 | 5470 |
| | 301 | 10 | 1.45 | 0.57 | 4585 |
| | 313 | 10 | 1.31 | 0.44 | 4143 |
| | 77 | 10 | 1.72 | 2.18 | 5439 |
| | 313 | 10 | 1.26 | 0.44 | 3984 |

*Ref. Term 1 Thermostat broken, continuous heat input but not constant temperature.

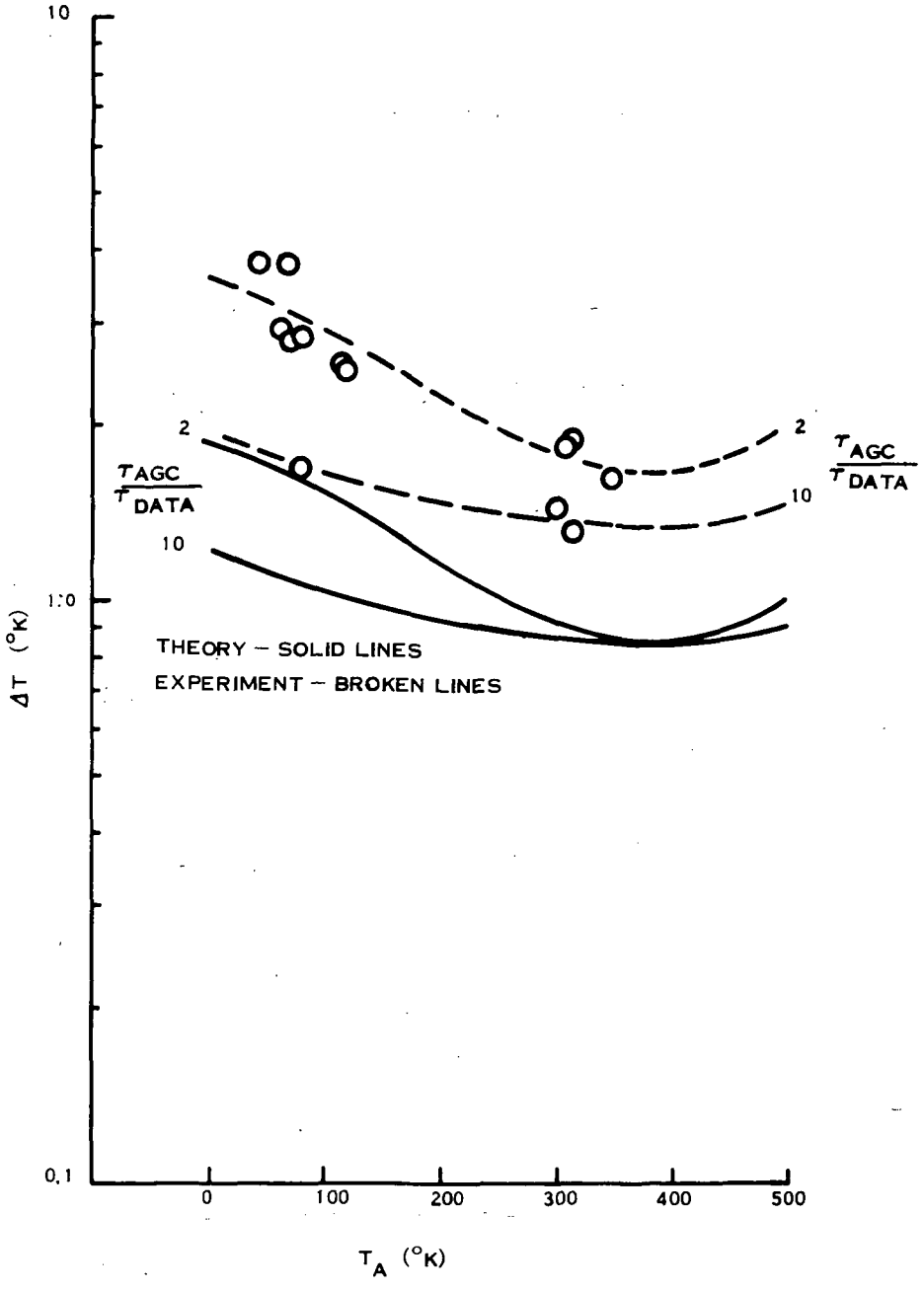


Figure 5-1. Minimum Detectable Signal - AAFE RADSCAT

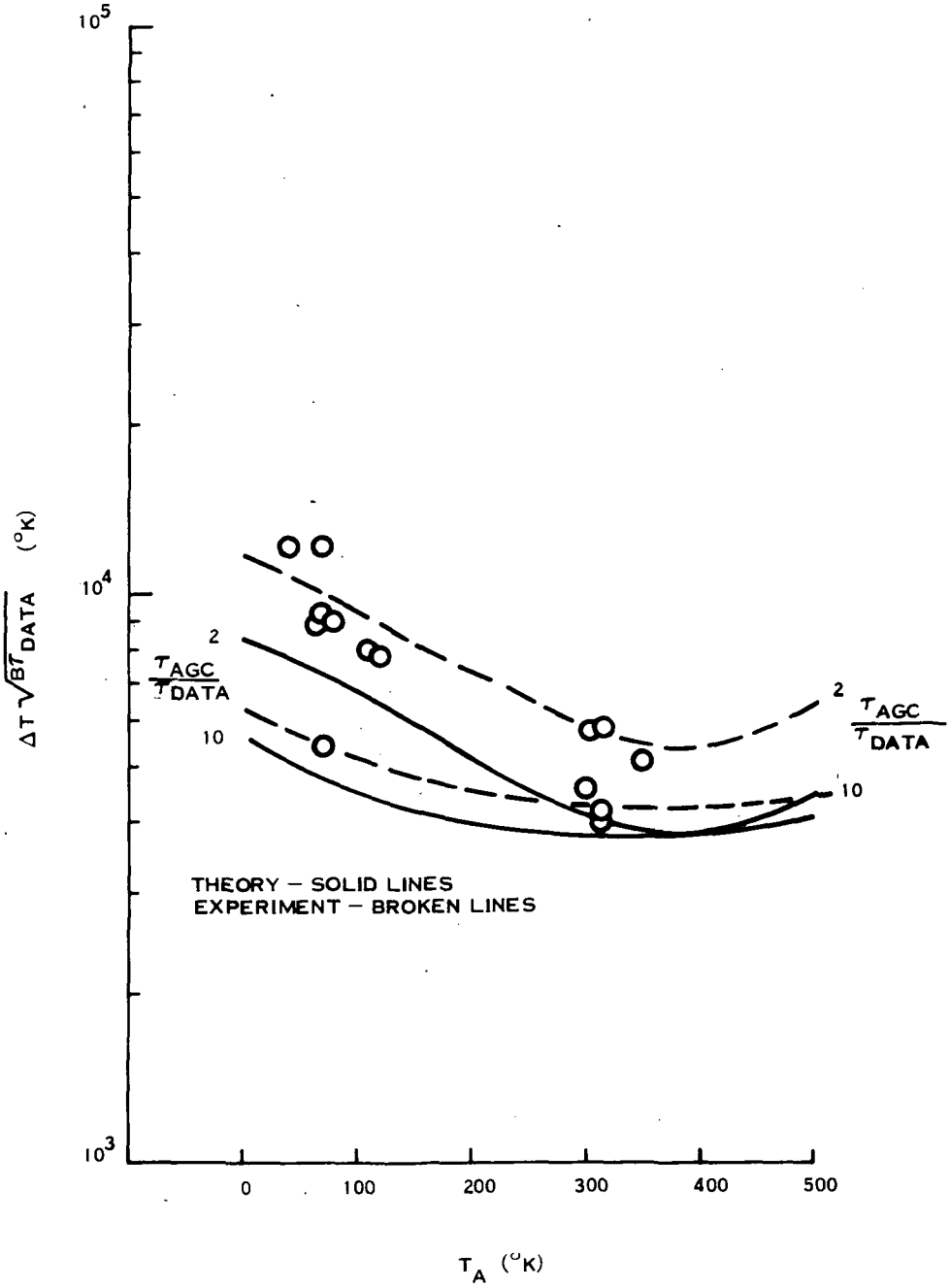


Figure 5-2. Sensitivity - AAFE RADSCAT

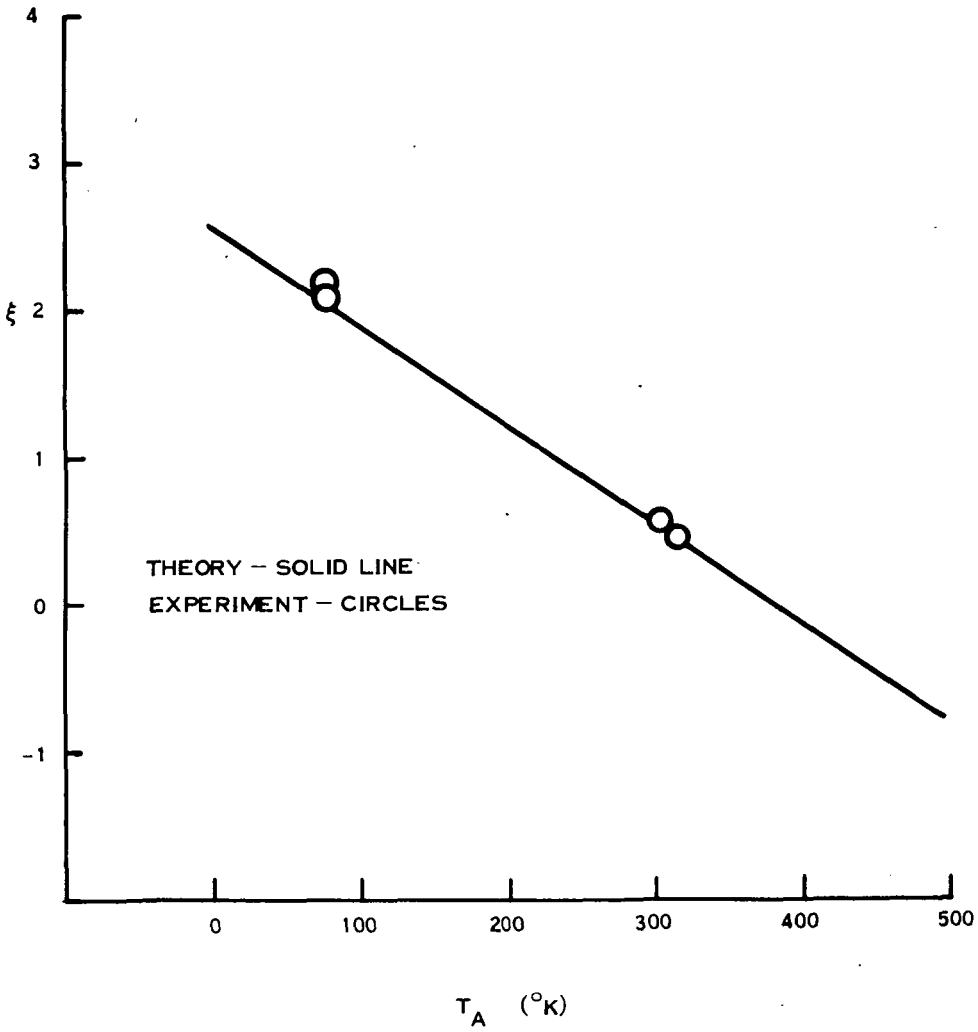


Figure 5-3. Normalized Radiometer Output ($\xi$) - AAFE RADSCAT

## 5.1 RADSCAT TESTS

Data on the RADSCAT instrument was collected under the direction of NASA Langley Research Center at Table Mountain, California. The antenna viewed clear sky and a uniform temperature microwave absorber in sequence. After the tests were completed, it was discovered that reference termination No. 1 (426$^{o}$K) was defective and was in excess of its rated temperature. It was also changing temperature since its thermostat was broken. The data presented, in Figure 5-1, however, shows that the resolution of the instrument does follow the theoretical trend with antenna temperature variation. The normalized radiometer output ($\xi$) is not computed for the Table Mountain data due to the fact that $T_{1e}$, for this series of tests, is in question and the accuracy of the tests is already questionable due to the variations in sky temperature and in the microwave absorber.

The tests at General Electric Space Division were conducted in a laboratory environment using commercial radiometer loads at 77$^{o}$K and 313$^{o}$K, and an uncontrolled ambient temperature (301$^{o}$K) waveguide termination. Several tests were conducted at each temperature and at least 60 data points were averaged over 60 seconds for each datum entered in Table 5-2. The fact that the 301$^{o}$K load was not controlled closely in temperature may be seen by comparing $\Delta T_{(301^{o}K)}$ with $\Delta T_{(313^{o}K)}$ in Figure 5-1, and observing that the uncontrolled load has a larger variation in temperature resolution. This same effect is felt to have occurred with the microwave absorber during the Table Mountain tests.

Finally, an experimental measurement of $\xi$, shown in Figure 5-3, was made and compared favorably with the theory. This indicated that the instrument is accurate when all loss and VSWR corrections are accounted for, using the expressions developed in this thesis.

# SECTION 6
# SUMMARY

A model was developed for the switching radiometer utilizing a continuous method of calibration. Sources of system degradation were identified and include losses and VSWR's in front of the receiver input. After computing the three modes of operation (Baseline Calibration, Normal Calibration, and Measurement Mode), expressions were developed for $\xi$, the normalized radiometer output; $\Delta T$, the minimum detectable signal (normalized RMS temperature fluctuation); $\Delta T \sqrt{B\tau_{DATA}}$, sensitivity (Figure of Merit); and accuracy (correction factors).

Specifically:

- The output of the radiometer is linear with input temperature and may be expressed in terms of the sum and the difference between the internal reference temperatures.
- The minimum detectable signal is a complex function of the system parameters as well as the input temperature, and for the RADSCAT timing sequence (with blanking) shows an improvement over previously published designs.
- The expression for the sensitivity of radiometers allows for the comparison of different radiometers without explicit correction for their different bandwidths and integration time constants as well as their physical circuit implementation.

- The accuracy of the CCR is influenced directly by all losses and reflection coefficients before the receiver input. Some corrections are negligible for low loss-low VSWR systems. However, in all cases, a correction factor exists which is a function of the components in the reference temperature portion of the radiometer.
- A practical application of the analysis developed herein was made using the AAFE RADSCAT.

The results compared favorably with the predicted performance of the instrument using the expressions developed herein. $\xi$ correlated extremely well. $\Delta T$ was several tenths of a degree Kelvin higher than predicted when measured in a laboratory. $\Delta T$ was also higher when measured during tests at Table Mountain, California. These differences are attributed to reference temperature errors both internal and external to the instrument.

## APPENDIX A

## NETWORK ANALYSIS FOR NOISE MEASUREMENT

Numerous references on Noise Measurement are available but the following is a summary of a National Bureau of Standards paper [18] applicable to radiometry.

Consider a general network (Figure A-1) with the following parameters:

| | |
|---|---|
| $\Gamma_S$, $\Gamma_L$, $\Gamma_1$, $\Gamma_2$ | Reflection coefficients |
| S | The two-port scattering matrix |
| $Z_M$, $Z_N$ | The characteristic line impedance |
| $P_{1d}$, $P_{2d}$ | Net power delivered across reference planes 1 and 2 respectively |
| 1, 2 | The reference planes |
| $Z_G$, $Z_L$ | The generator and load impedances respectively |

It may be shown [19] that the Scattering Matrix and the reflection coefficients are related at the reference planes by

$$\Gamma_1 = S_{11} + \frac{S_{12}\, S_{21}\, \Gamma_L}{1 - S_{22}\, \Gamma_L} \tag{A1}$$

Similarly,

$$\Gamma_2 = S_{22} + \frac{S_{12}\, S_{21}\, \Gamma_G}{1 - S_{11}\, \Gamma_G} \tag{A2}$$

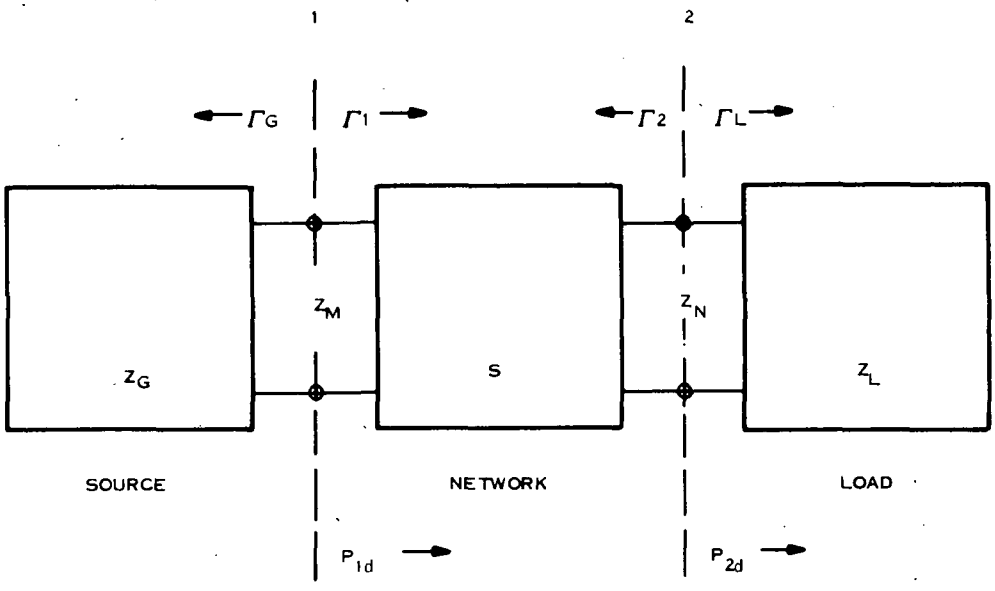


Figure A-1. General Network

Miller[20] defines four derived expressions of interest to the analysis. The first two are the mismatch factors M and N associated with the interface planes 1 and 2 respectively:

$$M \equiv \frac{(1 - |\Gamma_G|^2)(1 - |\Gamma_1|^2)}{|1 - \Gamma_G \Gamma_1|^2} \tag{A3}$$

$$N \equiv \frac{(1 - |\Gamma_L|^2)(1 - |\Gamma_2|^2)}{|1 - \Gamma_L \Gamma_2|^2} \tag{A4}$$

Next is the efficiency,

$$\eta \equiv \frac{P_{2d}}{P_{1d}} = \frac{Z_M/Z_N \, |S_{21}|^2 (1 - |\Gamma_L|^2)}{(1 - |\Gamma_1|^2) \, |1 - S_{22} \Gamma_L|^2} \tag{A5}$$

and fourth is $\alpha$, a ratio of the available power at the output to the power at the input:

$$\alpha \equiv \frac{P_{2a}}{P_{1a}} = \frac{M\eta}{N} = \frac{(Z_M/Z_N)\,|S_{21}|^2\,(1-|\Gamma_G|^2)}{(1-|\Gamma_2|^2)\,|1-S_{11}\,\Gamma_G|^2} \tag{A6}$$

where $P_{1d} = MP_{1a}$

$P_{2d} = NP_{2a}$

Of prime importance is the realization that both $\alpha$ and $\eta$ measure the lossiness of the two-port S and, if S is lossiness, then

$$\eta = 1 = \alpha \tag{A7}$$

Also $\alpha$ will be a direct measure of the noise contribution of the two-port to the output. Please note that, in general, $\alpha$ is independent of $\Gamma_L$, and $\eta$ is independent of $\Gamma_G$. Therefore, these expressions lend themselves to a method of writing convenient expressions for use in radiometer noise power analysis.

## APPENDIX B

## ANALYSIS OF NOISE GENERATION IN CASCADED MISMATCHED TWO-PORT NETWORKS

The noise generated in a cascade of unmatched two-ports will be develepod first from a simple model neglecting secondary reflections. Afterwards, the first order secondary reflections will be considered. For a more exact analysis see Mukaihata [21].

Consider Figure B-1, the model of a two-port, with a composite mismatched $R_{in}$, $R_{out}$ on each port and terminated on the input by a zero degree Kelvin $Z_o$ load, and on the output by a $Z_o$ load. The effective radiometric temperature at the output is computed as follows:

For simplicity of calculation, $C \leq L \leq 1$ where $L = 1$ indicates no loss (100 % transmission) and $L = 0$ indicates infinite loss (0% transmission).

Then,

$$T_{out} = 0^{o} + (1-L)\, T_o\, (1-R_{out})$$

Considering next the case of the first order reflections on the input,

$$T_{out} = 0^{o} + (1-L)\, T_o\, (R_{in}) + (1-L)\, T_o\, (1-R_{out})$$

$$= (1-L)\, (1 + R_{in})\, (1-R_{out})\, T_o$$

then,

$$T_{out} = (1-L)\, (1 + R_{in})\, (1 - R_{out} + R_{out}^{2} - R_{out}^{3})$$

For moderate VSWR, i.e., VSWR $\leq$ 2.0:1, $R \leq 0.11$,

$R^2 = 0.012$, and $R^2 >> R$

$$T_{out} = (1-L)\, (1 + R_{in})\, (1 - R_{out})\, T_o$$

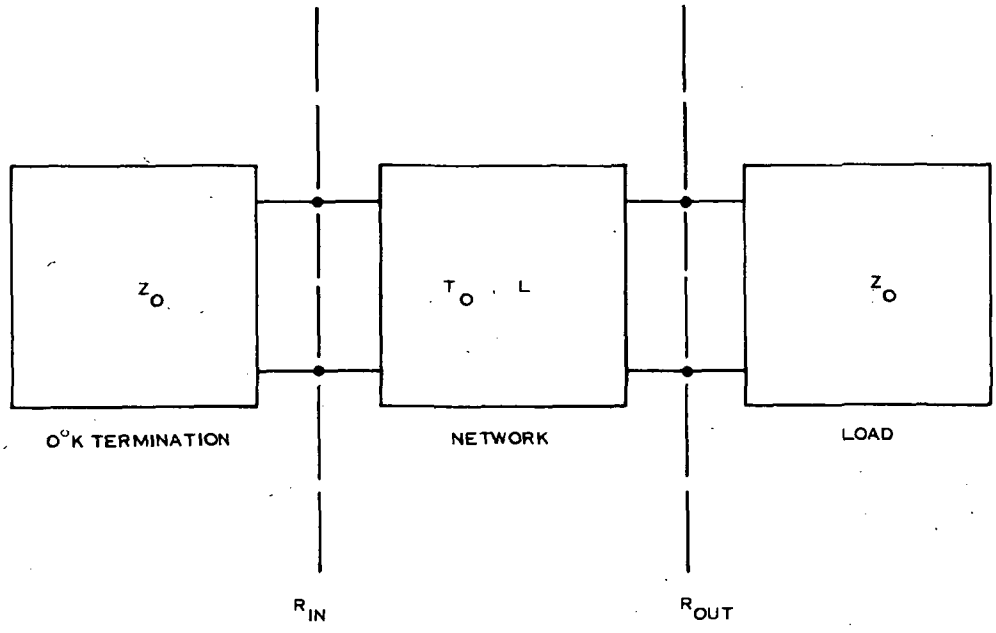


Figure B-1. Two-Port Model

For the purposes of the analysis, the effective radiometric temperature of a two-port is

$$T = (1-L)\,(1 + R_{in})\,(1 - R_{out})\,T_o$$

Extending this to a cascade of unmatched two-ports, with no power input to the cascade, and with different temperatures for each loss,

$$T_{out} = \sum_{i=1}^{n} T_i$$

$$T_{out} = \Bigg[ \cdots \Bigg| \Big[ \Big[ (1-L_1)\,R_1 L_1 + (1-L_1) \Big] \; T_{L_1} \Big] \; (1-R_2)\,L_2 + \Big[ (1-L_2)\,R_2 L_2 + (1-L_2) \Big] \; T_{L_2} \Big] \; (1-R_3)\,L_3 + \cdots \Bigg] \; (1-R_n)\,L_n + \Big[ (1-L_n)\,R_n L_n + (1-L_n) \Big] \; T_N \Bigg] \; (1-R_{n+1})$$

Simplifying,

$$T_{out} = \Big[ \cdots \Big[ \Big[ \Big[ (1-L_1)\ (1+R_1L_1) \Big] \quad T_{L_1} \quad (1-R_2)\ L_2 + \Big[ (1-L_2)\ (1+R_2L_2) \Big] \quad T_{L_2} \Big] \quad (1-R_3)\ L_3 + \cdots \Big] \quad (1-R_n)\ L_n + \Big[ (1-L_n)\ (1+R_nL_n) \Big] \quad T_N \Big] \quad (1-R_{n+1})$$

and for the same temperature, $T_o$,

$$T_{out} = \Big[ \cdots \Big[ \Big[ \Big[ (1-L_1)\ (1+R_1L_1) \Big] \quad (1-R_2)\ L_2 + \Big[ (1-L_2)\ (1+R_2L_2) \Big] \Big] \quad (1-R_3)\ L_3 + \cdots \Big] \quad (1-R_n)\ L_n + \Big[ (1-L_n)\ (1+R_nL_n) \Big] \Big] (1-R_n+1) \quad T_o$$

## REFERENCES


(1) Tomiyasu, Kiyo, "RADSCAT Literature with Annotations," PIR U-114F-EOS-111, General Electric Company, Space Division, Valley Forge, Pa., December 9, 1971.

(2) Classen, John P., "The AAFE RADSCAT Program at the University of Kansas, "Program Review Notes (Presented at Valley Forge Space Center), University of Kansas CRES, Lawrence, Kansas, October 1971.

(3) Dicke, R. H., "The Measurement of Thermal Radiation at the Microwave Frequencies," Rev. Sci. Instr., Vol. 17, pp 268-279, July 1946.

(4) Weinreb, S., "Advanced High Sensitivity Microwave Radiometers," 1969 Int'l Conf. on Microwires, Circuit Theory, and Information Theory, Tokyo (Summaries of Papers) Pt. 1, pp 95-96.

(5) Hach, J. P., "Proposal for a Continuously Calibrated Radiometer," Proceedings of the IEEE, Vol. 54, No. 12, pp. 2015-2016, December 1966.

(6) Hach, J. P., "A Very Sensitivity Airborne Microwave Radiometer Using Two Reference Temperatures," IEEE Transactions on Microwave Theory and Techniques, Vol. MTT-16, No. 9, pp 629-636, September 1968.

(7) Louapre, Merlin E., et al., "A High-Efficiency Electronically Scanned K-Band Phased Array for Space Borne Radiometric Applications," Proceedings of the IEEE Vol. 56, No. 11, pp 2010-2016, November 1968.

(8) Mumford, W. W., and Scheibe, E. H., Noise Performance Factors in Communications Systems, Horizon House-Microwave Inc., Dedham, Mass., p. 8, 1968.

(9) Vander Ziel, A., Noise, Prentice Hall, Englewood Cliffs, N. J., p. 9 1956.

(10) Dicke, R. H., Op Cit., pp 268-279.

(11) Vander Ziel, A., Op Cit, pp 336-337

REFERENCES (Cont)

(12) Vander Ziel, A., Op Cit, p. 5.

(13) Hach, J. P., Op Cit, p. 631, equation (14)

(14) Hach, J. P., Op Cit, p. 631, equation (17).

(15) Hach, J. P., Op Cit, p. 631, equation (21)

(16) Tomiyasu, Kiyo, "An Introduction to Microwave Radiometers," PIR U-114F-EOS-034, General Electric Company Space Division, Valley Forge, Pa., July 6, 1971.

(17) Hach, J. P., Op Cit, p. 634.

(18) Miller, C. K. S., Daywitt, W. C., and Arthur, M. G., "Noise Standards, Measurements, and Receiver Noise Definition," Proc. IEEE Vol. 55, No. 6, pp 865-877.

(19) Kerns, D. M., and Beatty, R. W., Basic Theory of Waveguide Junctions and Introductory Microwave Network Analysis, Permgamon Press, Oxford, pp 42, 1967.

(20) Miller, C. K. S., et al., Op Cit, p. 865.

(21) Mukaihata, Tadao, "Applications and Analysis of Noise Generation in N-Cascaded Mismatched Two-Port Network," IEEE Transactions on Microwave Theory and Techniques Vol. MTT-16, No. 9, pp 699-708, September 1968.

NATIONAL AERONAUTICS AND SPACE ADMINISTRATION
WASHINGTON, D.C. 20546

OFFICIAL BUSINESS
PENALTY FOR PRIVATE USE $300

SPECIAL FOURTH-CLASS RATE
BOOK

POSTAGE AND FEES PAID
NATIONAL AERONAUTICS AND
SPACE ADMINISTRATION
451

U.S.MAIL

POSTMASTER : If Undeliverable (Section 158 Postal Manual) Do Not Return

*"The aeronautical and space activities of the United States shall be conducted so as to contribute . . . to the expansion of human knowledge of phenomena in the atmosphere and space. The Administration shall provide for the widest practicable and appropriate dissemination of information concerning its activities and the results thereof."*

—NATIONAL AERONAUTICS AND SPACE ACT OF 1958

# NASA SCIENTIFIC AND TECHNICAL PUBLICATIONS

TECHNICAL REPORTS: Scientific and technical information considered important, complete, and a lasting contribution to existing knowledge.

TECHNICAL NOTES: Information less broad in scope but nevertheless of importance as a contribution to existing knowledge.

TECHNICAL MEMORANDUMS: Information receiving limited distribution because of preliminary data, security classification, or other reasons. Also includes conference proceedings with either limited or unlimited distribution.

CONTRACTOR REPORTS: Scientific and technical information generated under a NASA contract or grant and considered an important contribution to existing knowledge.

TECHNICAL TRANSLATIONS: Information published in a foreign language considered to merit NASA distribution in English.

SPECIAL PUBLICATIONS: Information derived from or of value to NASA activities. Publications include final reports of major projects, monographs, data compilations, handbooks, sourcebooks, and special bibliographies.

TECHNOLOGY UTILIZATION PUBLICATIONS: Information on technology used by NASA that may be of particular interest in commercial and other non-aerospace applications. Publications include Tech Briefs, Technology Utilization Reports and Technology Surveys.

***Details on the availability of these publications may be obtained from:***

**SCIENTIFIC AND TECHNICAL INFORMATION OFFICE**

**NATIONAL AERONAUTICS AND SPACE ADMINISTRATION**

**Washington, D.C. 20546**